Row	Height	ID	25%	50%	75%	OD
1	0.000	-28.324	-18.299	-12.16	-6.2006	-0.02118
101	0.350	-18.794	-12.495	-6.6068	-1.3662	3.655
201	0.630	-17.838	-10.518	-4.4065	-0.47664	2.0799
301	0.854	-20.517	-12.968	-5.9018	-0.87378	-1.5355
401	1.034	-19.663	-11.831	-5.2884	0.22693	1.4602
501	1.178	-17.203	-10.587	-0.51546	16.326	21.019
601	1.293	-8.023	-2.2049	10.461	32.658	37.289
701	1.442	4.7776	9.5574	24.903	38.177	54.089
801	1.591	13.252	18.569	35.278	52.808	66.517
901	1.740	16.001	22.017	39.194	62.945	75.001
1001	1.889	15.857	23.14	40.235	64.335	74.874
1101	2.038	12.629	23.76	41.263	58.673	66.777
1201	2.187	10.061	25.095	39.628	49.272	55.012
1301	2.336	11.161	24.955	35.646	38.588	37.57
1401	2.485	17.623	24.541	31.309	28.654	24.693
1501	2.634	27.264	24.647	26.511	19.508	17.468
1601	2.783	35.465	28.75	27.109	14.597	16.305
1701	2.933	39.949	34.666	31.396	15.64	12.404
1801	3.082	39.547	36.368	37.156	24.257	1.4483

Table 12: *Nodal stress for 49.6° nozzle at the downhill location. The weld location is shown by the shaded row.*
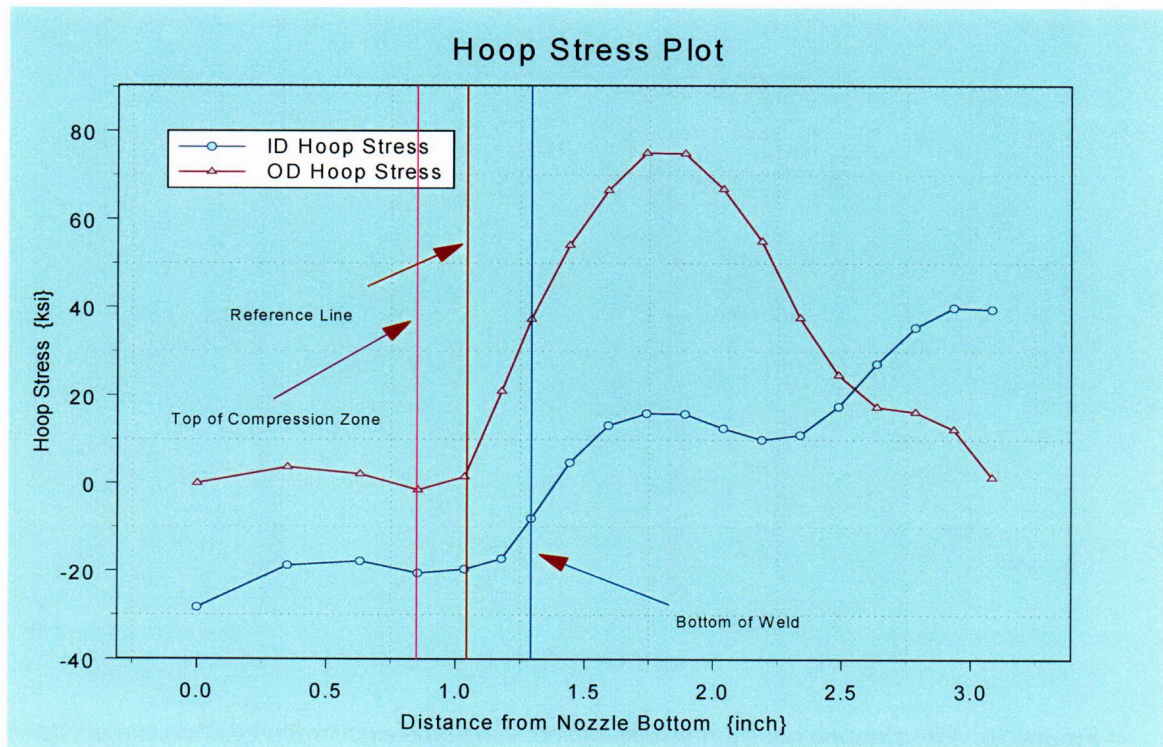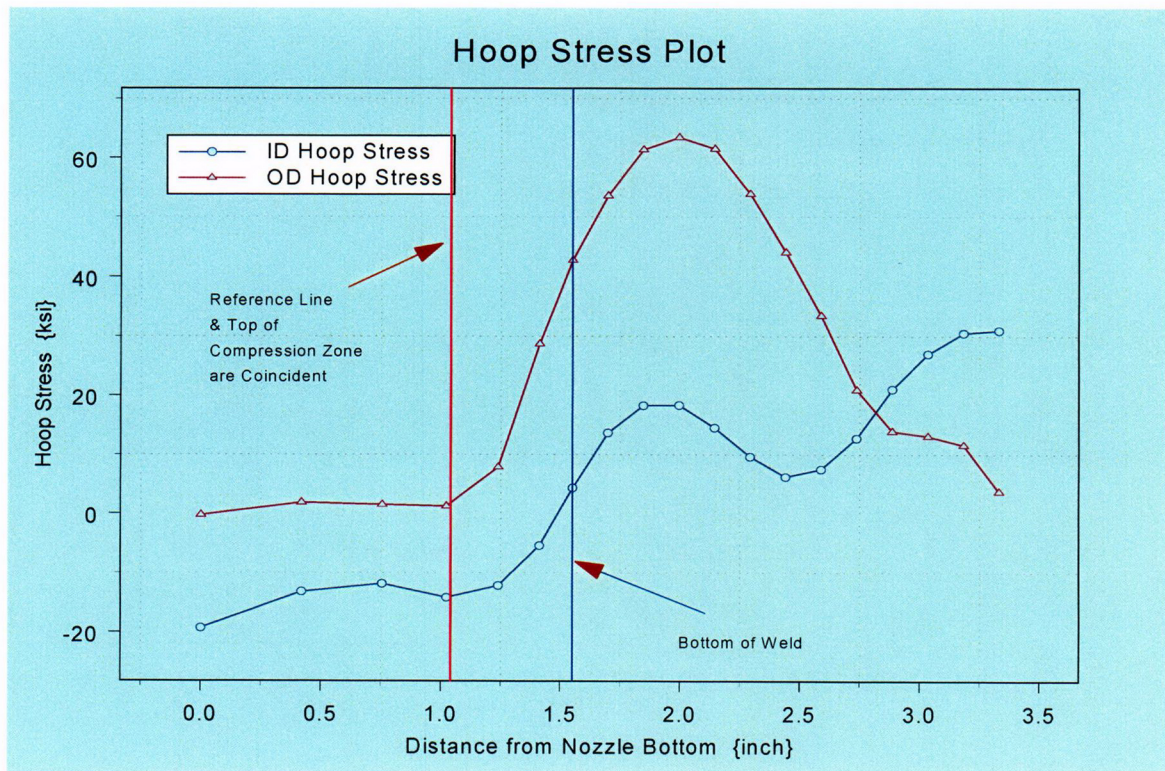

Figure 19: *Plot showing hoop stress distribution along tube axis for the 49.6° nozzle at the downhill location. The top of compressive zone, the reference line, and the bottom of the weld are shown.*

C15

Row	Height	ID	25%	50%	75%	OD
10001	0	-19.301	-12.523	-8.3043	-4.3142	-0.28909
10101	0.41913	-13.153	-8.5716	-4.6802	-1.2548	1.8343
10201	0.75491	-11.834	-6.958	-2.6848	0.027936	1.4633
10301	1.0239	-14.146	-8.3146	-3.1681	1.1025	1.2206
10401	1.2394	-12.132	-6.552	0.003002	5.7801	7.8584
10501	1.4121	-5.3804	-2.4127	7.4976	23.29	28.718
10601	1.5504	4.3312	6.4775	17.842	35.67	42.747
10701	1.6988	13.644	15.667	27.164	40.65	53.563
10801	1.8473	18.304	21.201	32.424	50.345	61.379
10901	1.9957	18.316	22.292	34.208	53.258	63.464
11001	2.1442	14.517	21.816	35.085	51.479	61.5
11101	2.2926	9.6239	20.816	34.508	47.885	53.875
11201	2.441	6.1777	19.919	32.257	40.249	44.059
11301	2.5895	7.4871	19.244	30.005	33.466	33.498
11401	2.7379	12.725	18.544	26.491	26.271	20.889
11501	2.8864	21.018	19.128	23.312	19.922	13.905
11601	3.0348	27.04	22.243	23.901	17.166	13.045
11701	3.1833	30.565	26.038	26.927	19.252	11.52
11801	3.3317	31.022	26.941	29.307	23.991	3.6688

Table 13: *Nodal stress for 49.6° nozzle at the 22.5° rotated from the downhill location. The weld location is shown by the shaded row.*
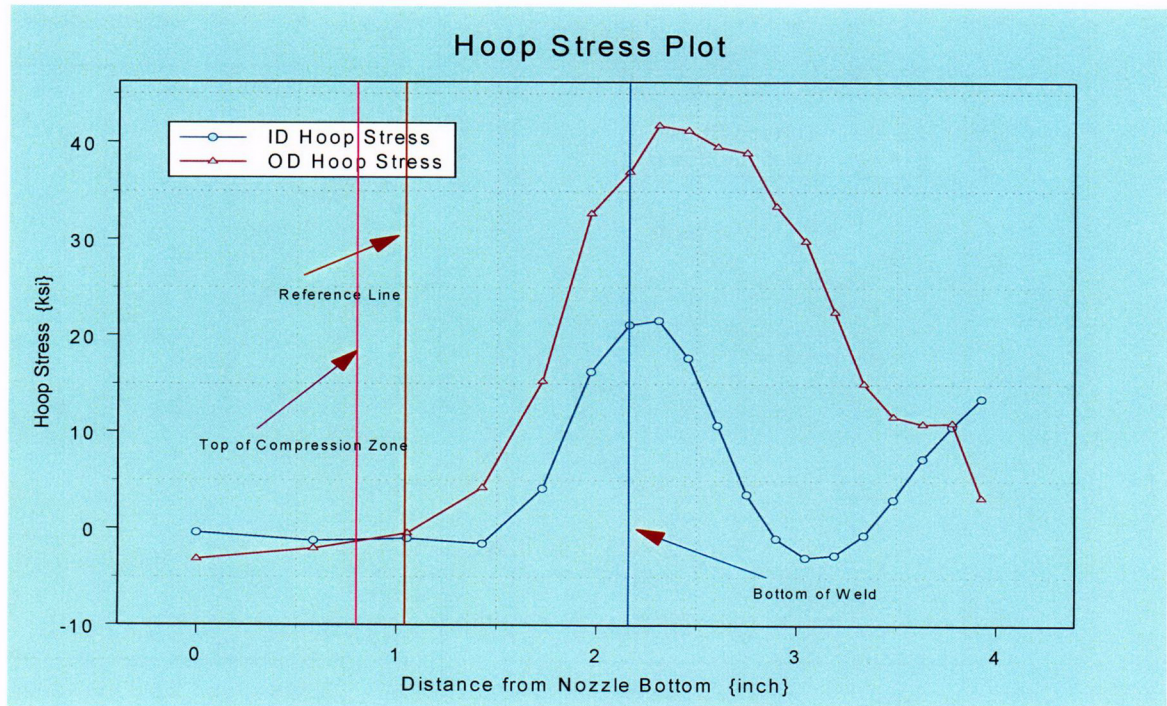

Figure 20: *Plot showing hoop stress distribution along tube axis for the 49.6° nozzle at 22.5° rotated from the downhill location. The top of compressive zone, the reference line, and the bottom of the weld are shown.*

Row	Height	ID	25%	50%	75%	OD
20001	0	-0.41426	-1.3595	-1.8423	-2.3694	-3.1566
20101	0.58479	-1.2562	-1.4879	-1.714	-1.9503	-2.0734
20201	1.0533	-1.0226	0.22345	0.34713	0.51562	-0.49543
20301	1.4286	-1.5585	0.62217	2.583	4.8953	4.258
20401	1.7293	4.1652	4.3149	8.8598	13.38	15.252
20501	1.9702	16.258	12.541	16.926	28.26	32.667
20601	2.1632	21.131	17.131	20.087	34.279	36.98
20701	2.3099	21.593	19.093	21.933	34.049	41.718
20801	2.4567	17.702	17.82	22.18	34.468	41.213
20901	2.6034	10.688	14.251	21.112	33.319	39.555
21001	2.7502	3.5924	10.953	19.959	31.013	38.939
21101	2.8969	-0.98491	8.7362	18.339	28.346	33.446
21201	3.0437	-2.9447	7.0211	18.062	25.996	29.853
21301	3.1905	-2.6882	5.4512	16.967	23.256	22.48
21401	3.3372	-0.60958	5.0995	15.966	21.557	15.04
21501	3.484	3.0879	4.9369	15.116	19.082	11.629
21601	3.6307	7.3077	6.878	15.74	18.42	10.876
21701	3.7775	10.628	9.0825	17.263	20.586	10.946
21801	3.9242	13.502	11.129	17.922	23.742	3.2671

Table 14: *Nodal stress for 49.6° nozzle at the 45° rotated from the downhill location. The weld location is shown by the shaded row.*
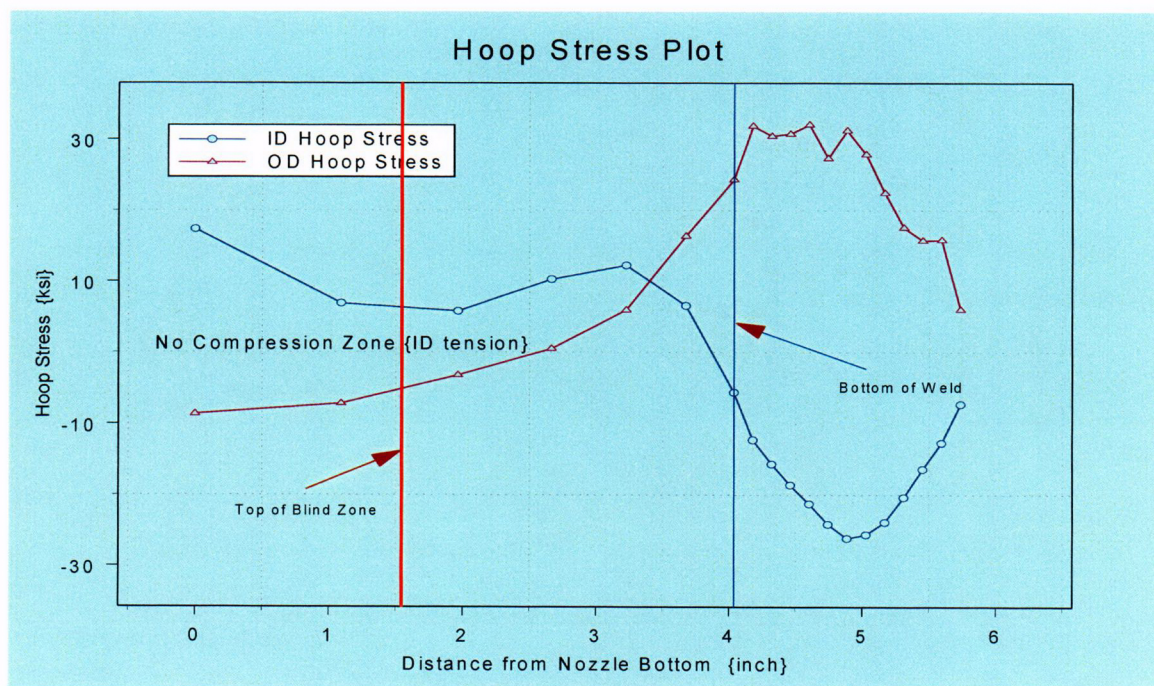

Figure 21: *Plot showing hoop stress distribution along tube axis for the 49.6° nozzle at 45° rotated from the downhill location. The top of compressive zone, the reference line, and the bottom of the weld are shown.*

Row	Height	ID	25%	50%	75%	OD
40001	0.000	17.354	8.1856	2.2843	-3.0637	-8.6374
40101	1.091	6.8916	1.4705	-2.2239	-5.4445	-7.1995
40201	1.964	5.7811	2.359	0.75379	-0.955	-3.2318
40301	2.664	10.289	7.1481	5.3241	3.4277	0.49388
40401	3.225	12.243	7.028	6.8287	7.2436	5.9517
40501	3.674	6.5788	4.6585	5.8654	12.453	16.377
40601	4.034	-5.6212	-1.2955	4.1843	17.859	24.278
40701	4.176	-12.251	-6.006	2.7409	20.517	31.88
40801	4.318	-15.641	-9.1309	2.2005	21.496	30.446
40901	4.459	-18.614	-11.785	1.3186	20.216	30.786
41001	4.601	-21.257	-13.548	0.57363	19.393	32.088
41101	4.743	-24.142	-14.864	0.3385	19.564	27.322
41201	4.884	-26.133	-15.268	-0.15264	17.776	31.244
41301	5.026	-25.615	-14.158	0.78773	15.555	27.871
41401	5.167	-23.831	-12.25	1.7886	16.579	22.427
41501	5.309	-20.331	-10.681	3.0892	16.489	17.553
41601	5.451	-16.345	-8.6522	4.4543	17.912	15.75
41701	5.592	-12.679	-6.5122	5.5067	16.075	15.827
41801	5.734	-7.2577	-2.477	7.8649	19.847	6.0174

Table 15: *Nodal stress for 49.6° nozzle at the (Mid-Plane) 90° rotated from the downhill location. The weld location is shown by the shaded row.*
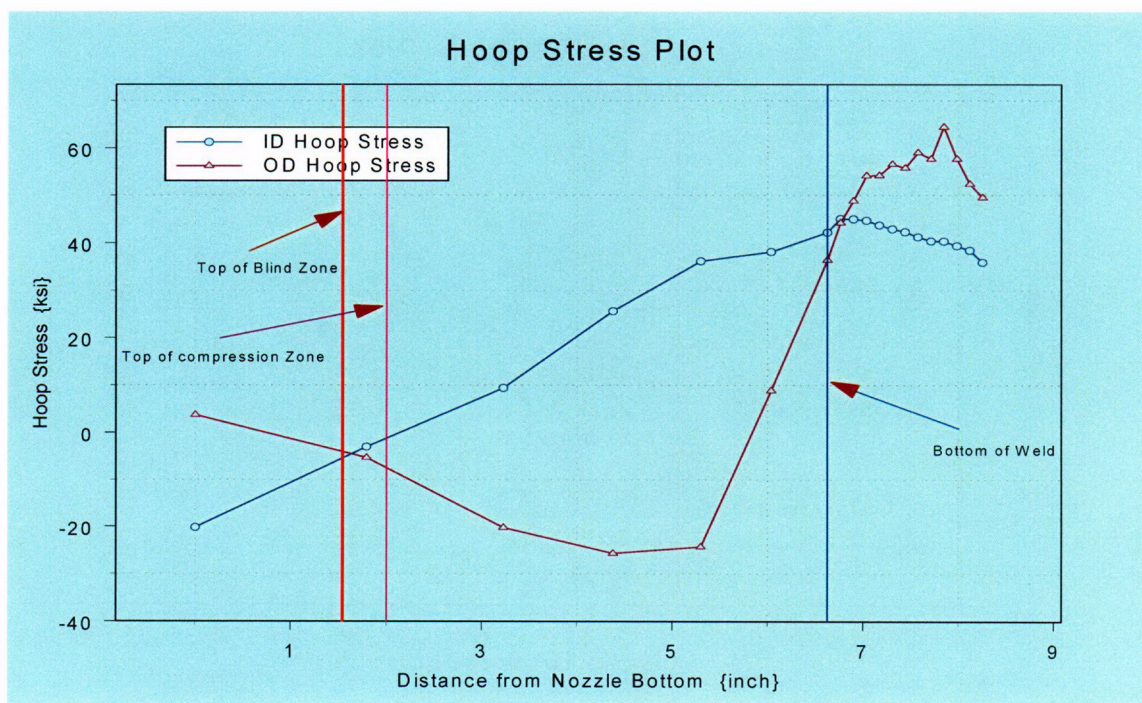

Figure 22: *Plot showing hoop stress distribution along tube axis for the 49.6° nozzle at (Mid-Plane) 90° rotated from the downhill location. The top of blind zone, and the bottom of the weld are shown. There is no compression zone since the ID is in tension.*

C18

Row	Height	ID	25%	50%	75%	OD
80001	0.000	-20.175	-11.45	-5.9403	-1.1628	3.7037
80101	1.792	-3.0237	-4.3776	-5.4433	-5.5114	-5.3415
80201	3.228	9.3983	12.134	-0.25796	-12.622	-20.232
80301	4.378	25.65	24.71	14.577	-15.299	-25.689
80401	5.299	36.179	33.787	26.287	-5.9249	-24.306
80501	6.037	38.106	35.028	31.43	21.215	8.834
80601	6.628	42.186	38.102	36.248	40.684	36.405
80701	6.764	45.067	42.217	42.736	47.553	44.235
80801	6.899	44.968	43.606	46.007	49.995	48.803
80901	7.035	44.695	44.12	47.021	51.043	54.113
81001	7.170	43.723	43.973	47.639	50.172	54.17
81101	7.305	42.926	43.816	47.515	52.325	56.546
81201	7.441	42.312	43.142	47.497	51.329	55.754
81301	7.576	41.252	42.489	47.751	53.141	58.971
81401	7.712	40.403	41.864	46.936	54.111	57.676
81501	7.847	40.359	40.735	47.685	56.669	64.401
81601	7.982	39.39	39.72	46.452	53.712	57.649
81701	8.118	38.459	37.5	43.25	47.79	52.344
81801	8.253	35.922	35.062	36.626	38.139	49.538

Table 16: *Nodal stress for 49.6° nozzle at the (Uphill) 180° rotated from the downhill location. The weld location is shown by the shaded row.*

Figure 23: *Plot showing hoop stress distribution along tube axis for the 49.6° nozzle at (Uphill) 180° rotated from the downhill location. The top of the compression zone, the top of blind zone, and the bottom of the weld are shown.*

C19

The nodal stress data presented in the previous pages are the data imported into the respective Mathcad worksheet (discussed later) for further processing to obtain the pertinent stress distributions required for the fracture mechanics analysis. The processing of the nodal stress data is described in Section 4.

3.0 Analytical Basis for Fracture Mechanics and Crack Growth Models

Fracture Mechanics Models

Surface Crack

The mean radius-to-thickness ratio (R_m/t) for the CEDM nozzle was about 1.7. The fracture mechanics equation used in the proposed revision to the ASME Code Section XI is based on the solution from Reference 6. This solution is valid for an outside radius-to-thickness ("R_o/t") ratio from 4.0 to 10.0. The CEDM nozzle "R_o/t" ratio is lower (3.06), indicating that the CEDM nozzle is a thicker wall cylinder than those considered in Reference 6. Therefore, the fracture mechanics formulations presented in Reference 7 were chosen (the applicable "R_m/t" ratio is from 1.0 to 300.0).

The stress intensity factor (SIF) for the postulated crack under an arbitrary stress distribution was obtained from Reference 7. The model was for both an internal and external part through-wall surface crack subjected to an arbitrary stress distribution. This model is valid for a ratio of mean radius (R_{mean})-to-thickness (t) between 1.0 and 300.0. Since the ratio for the CEDM nozzle is about 1.7, this model is considered applicable.

The equation for the SIF for the deepest point of the crack is given as [7]:

$$K_I = (\frac{\pi}{Q}a)^{0.5} * [\sum_{i=0}^{3} \sigma_i G_i]$$

Where:

K_I = SIF {ksi√in.}

Q = Crack shape factor, defined as

$$Q = 1 + 1.464 * (\frac{a}{c})^{1.65} \quad \text{when a/c} \leq 1.0 \text{ and,}$$

$$Q = 1 + 1.464 * (\frac{c}{a})^{1.65} \quad \text{when a/c} > 1.0$$

a = Crack depth {inch}

σ_i = *Coefficients of the stress polynomial describing the hoop stress variation through the crack depth. Describes the power loading on the crack face.*

G_i = *Stress Intensity Correction Factors (SICF), which are provided in tables in Reference 7.*

In Reference 7 SICF is presented for both the depth point of the crack ("a-tip") and for the surface point of the crack ("c-tip"). Separate tables are provided for the internal (ID) and external (OD) surface cracks. In addition the values are provided in association with the R_m/t ratio, a/c ratio (crack aspect ratio), and a/t ratio (normalized crack depth). The SICF tables are large and a suitable interpolation scheme is necessary to obtain proper coefficients dependent on crack size and shape for a given cylindrical geometry. Selected SICF from the tables for internal cracks for two different R_m/t ratios and a/c ratios are presented in Figure 24 below.
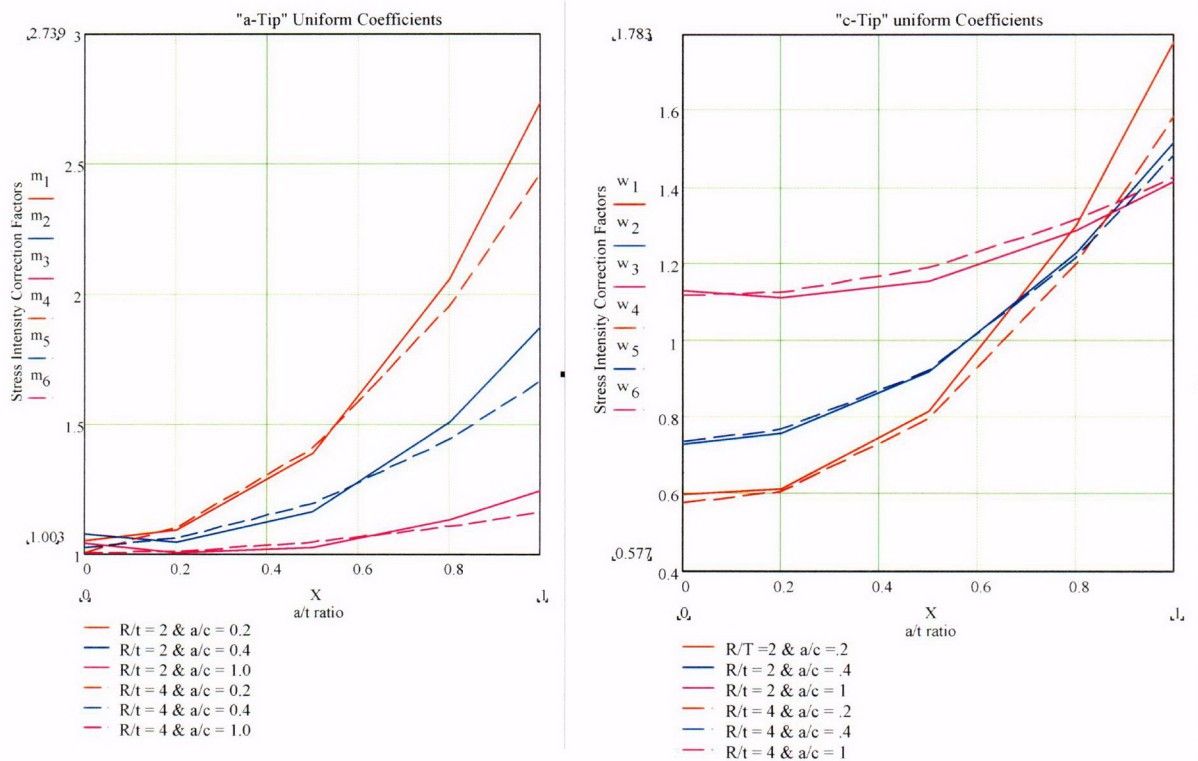
Figure 24: *SICF shown as a function of normalized crack depth for the "a-tip" (left figure) and the "c-tip" right figure. These figures show that simple linear interpolation would not provide accurate coefficients. These figures also show that a proper R_m/t is essential to provide a reasonably accurate estimate of the SIF.*

The figure above shows two features that are significant;

1) The interpolation used to obtain the SICF must be carefully performed such that the value accurately represents the crack geometry. This is accommodated by selecting a suitable order for the polynomial prior to performing an interpolation to obtain the specific value. This aspect is discussed in further detail in the section describing the analysis method.

2) The correct R_m/t ratio is essential for obtaining a reasonably accurate estimate of the SIF. Using a higher ratio will tend to underestimate the SIF and hence under predict the crack growth.

Both these features have been considered in the development of the analysis model such that a reasonable, yet conservative, estimate of the SIF is obtained.

Through-Wall Axial Crack

The analysis for a through-wall axial crack was evaluated using the formulation of Reference 8. This formulation was chosen since the underlying analysis was performed considering thick-wall cylinders that had "R_o/t" ratio in the range of the application herein. The analysis used the outside surface (OD) as the reference surface and, hence, the same notation is used here.

It was noted in Reference 8 that the formulations based on thin shell theory do not consider the complete three-dimensional nature of the highly localized stress distribution. This would be the case for the residual stress distribution from welding. The nonlinear three-dimensional stress distribution coupled with shell curvature must be properly addressed to account for the material behavior at the crack tip, which controls the SIF, such that the SIF is not underestimated. The information presented in Reference 8 compared the results from formulations derived using thin shell theory and those derived using thick shell formulation, these results highlighted the need to use thick shell based formulation for situations such as the current application to CEDM nozzle through-wall axial cracks.

The formulation provides the correction factors, which account for the "R_o/t" ratio and crack geometry (λ), that are used to correct the SIF for a flat plate solution subjected to similar loadings. The correction factors were given for both "extension" and "bending" components. The flat plate solutions for both membrane and bending loads were to be used to obtain the applied SIF. The formulations for SIF were given as [8]:

$$K_{outer} = \{ A_e + A_b \} * K_p \quad \text{for the OD surface;}$$

and,

$$K_{Inner} = \{A_e - A_b\} * K_p \text{ for the ID surface;}$$

where:

   A_e and A_b are the "extension" and "bending" components; and,

   K_p is the SIF for a cracked Flat Plate subject to the same boundary condition and loading as the cracked cylinder.

The flat plate SIF solutions are written as:

$$K_{p-Membrane} = \sigma_h * \sqrt{\pi * l} \text{ for membrane loading, and}$$

$$K_{p-Bending} = \sigma_b * \sqrt{\pi * l} \text{ for bending loading.}$$

Where:

   σ_h and σ_b are the membrane and bending stresses and "l" is one-half the crack length.

The reference surface used in the evaluation was the OD surface. The stresses at the ID and OD at the axial elevation of interest were decomposed into membrane and bending components as follows:

$$\sigma_h = \frac{\sigma_{res-OD} + \sigma_{res-ID}}{2} \text{ for membrane loading; and}$$

$$\sigma_b = \frac{\sigma_{res-OD} - \sigma_{res-ID}}{2} \text{ for bending loading.}$$

where:

   σ_{res-OD} is the stress (residual+operating) on the OD surface; and,

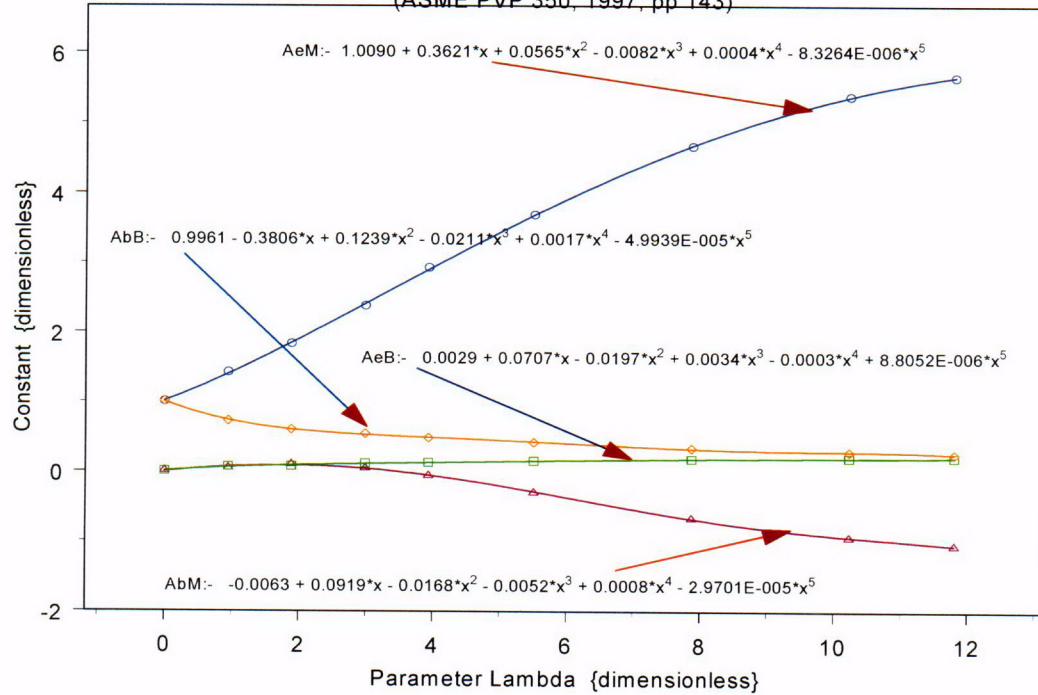   *σ_{res-ID} is the stress (residual+operating) on the ID surface.*

The data presented in the tables in Reference 8 for determining the A_e and A_b components were curve fit using a fifth order polynomial such that they could be calculated knowing the parameter λ, which is defined as [8]:

$$\lambda = \{[12 * (1 - v^2)]^{0.25} * \frac{l}{(R * t)^{0.5}}$$

where v is Poisson's ratio and R is the mean radius.

The data obtained from the tables in Reference 8 were curve fit using a fifth order polynomial. The curve fitting was accomplished using Axum 7 [9]. The curve fit results for the components are presented in Figure 25 below.

Extension and Bending Constants for Throughwall Axial Flaws R/t = 3.0

(ASME PVP 350, 1997; pp 143)

AeM:- $1.0090 + 0.3621*x + 0.0565*x^2 - 0.0082*x^3 + 0.0004*x^4 - 8.3264E-006*x^5$

AbB:- $0.9961 - 0.3806*x + 0.1239*x^2 - 0.0211*x^3 + 0.0017*x^4 - 4.9939E-005*x^5$

AeB:- $0.0029 + 0.0707*x - 0.0197*x^2 + 0.0034*x^3 - 0.0003*x^4 + 8.8052E-006*x^5$

AbM:- $-0.0063 + 0.0919*x - 0.0168*x^2 - 0.0052*x^3 + 0.0008*x^4 - 2.9701E-005*x^5$

Constant {dimensionless} (vertical axis)

Parameter Lambda {dimensionless} (horizontal axis)

Figure 25: *Curve fit equations for the "extension and "bending" components in Reference 8. Tables 1c and 1d for membrane loading and Tables 1g and 1h for bending loading of Reference 8 were used.*

Crack Growth Model

To evaluate the potential for crack growth due to PWSCC, the crack growth rate equation from EPRI-MRP 55 [10] was used. The crack growth rate as a function of the SIF with a correction for temperature effects is given as [10]:

$$\frac{da}{dt} = \exp[-\frac{Q_g}{R}(\frac{1}{T} - \frac{1}{T_{ref}})]\alpha(K - K_{th})^{\beta}$$

Where:

da/dt = crack growth rate at temperature T {m/s}

CZI

Q_g = *thermal activation energy for crack growth {31.0 kcal/mole}*

R = *universal gas constant {1.103x 10^{-3} kcal/mole-°R}*

T = *absolute operating temperature at crack tip {°R}*

T = *absolute reference temperature for data normalization {1076.67 °R}*

a = *crack growth amplitude {2.67x10^{-12}}*

K = *crack tip SIF {Mpa√m}*

K_{th} = *threshold SIF for crack growth {MPa√m}*

β = *exponent {1.16}*

The above equation represents the seventy-fifth percentile curve. Since the PWSCC crack growth of interest is in the primary water, this model would provide a reasonably conservative crack growth.

4.0 Method of Analysis

Mathcad Worksheet Format

The analytical scheme was developed using Mathcad [11] which facilitates calculations (including recursive) in a logical manner. Appendix B provides annotated versions of the three sets of worksheets used in the current analysis. The three sets are for the ID surface crack, the OD surface crack and for the through-wall crack. In the paragraphs below the general approach used to develop the worksheet is presented.

The first part of the worksheet is common to all three sets and requires the proper identification for the analysis being performed. In this region the component and the reference location in that component are identified. Immediately below the identification entry are the geometric landmark entries. For the surface cracks three entries are required and these are:

1)   The location of a reference line (e.g. blind zone location) referenced to the nozzle bottom {Ref$_{Point}$}.

2)   The location of the crack with respect to the reference line (Upper crack tip at the reference line, center of crack at the reference line or lower crack tip at the reference line) {Val};

3)   The location of the bottom of the weld measured upwards from the nozzle bottom {UL$_{Strs.Dist}$}.

For the through-wall crack the location of the crack upper tip is always at the reference line, while the two other land mark entries are similar to that for the surface crack. This completes the entries on the first page of the worksheet.

The second page of each Mathcad worksheet contains the inputs for crack dimensions, tube geometry, internal pressure, years of operation, iteration limit, operating temperature, and the constants for the PWSCC crack growth parameters. It should be noted that the crack growth is performed using metric units; hence, those constants are required to be in metric units. The remainder of this sheet does not require user input. The calculation shown is simple arithmetic to determine the values necessary for the analysis.

The third page of each worksheet is designed to import the entire nodal stress data from the Excel spreadsheet provided by Dominion Engineering (described earlier). After the required data has been imported, the graph below the data table depicts the ID and OD stress distributions along the axial length of the nozzle. This graph is needed to aid in the selection of the nodal stress data to be used in the subsequent analysis. Once the data needed for the evaluation has been selected, it is pasted onto the third sheet at a variable defined as "Data". No further user input is required. The worksheets presented in Appendix C reflect this design.

Determination of Stress Field (Distributions)

The first step in the analysis is to develop the appropriate stress distribution to be used in the determination of the SIF. This is needed because the SIF formulation is based on use of a uniform stress distribution along the length of the tube. However, the stress field at the bottom portion of the nozzle, starting from the nozzle bottom, increases in magnitude as the bottom of the weld is approached. Consequently, if an assumed crack located in the vicinity of the reference line were to grow by PWSCC, it would be subjected to an increasing stress field. Thus, to use the stress distribution at the initial crack location would lead to an underestimate of the SIF since the SIF is directly proportional to the applied stress. In order to obtain a reasonably representative SIF under the prevailing stress field variation, a moving average scheme was developed. This scheme is as follows:

1) For the initial crack location the stress distribution at the two crack tips (lower and upper) and the crack center are averaged to produce an average stress field that is applied to the crack. It is this stress distribution that is used to ascertain whether there exists a potential for PWSCC crack growth. This method is considered reasonable since it is similar to the superposition principle used in finite element based SICF determination.

2) The remaining portion of the nozzle extending from the upper crack tip to the bottom of the weld is divided into twenty (20) equal segments.

3) The stress distribution in the first segment, above the upper crack tip, is an arithmetic average of the first three initial crack region distribution (Lower tip, center of crack and the upper tip) plus the distribution in the first segment. Thus, when the crack enters the first segment the magnitude of the stress distribution is appropriately increased to account for the increased applied stress. Similarly, as the crack progresses upward to the weld bottom through the various segments, the applied stress distribution is adjusted accordingly. The small extent of the length between the reference

line and the bottom of the weld can be sufficiently accommodated by the twenty-segment characterization.

To accomplish this averaging scheme, the nodal stresses at the five (5) nodal locations through the tube thickness and its variation along the length of the nozzle are individually regressed with a third order polynomial. Hence, it is important to ensure that the axial distribution can be described by a third-order polynomial. The regression is performed along the nozzle axis at each of the five (5) locations individually. The result of the regression provides the spatial coefficients required to describe the stress distribution. The nodal stress data representing the region of interest, from the nozzle bottom to an elevation just above the bottom of the weld, is selected. In this manner, it is expected that proper representation of the stress distribution, pertinent to crack initiation and growth, can be accurately described.

An example of this approach is presented in Figure 26 below. In this example, the stress at the ID and the OD locations were selected from a typical set of nodal stress data. The graphs immediately below show the individual stress distribution and the result from the third-order polynomial fit. In the first set, the entire data set from the bottom of the nozzle to the top of the J-weld was used. The regression curve shows that the general trend is captured; however, the fit in localized regions are not accurate representation of the original data. Significant variation that might cause errors in the determination of the SIF could occur, which in turn could lead to an inaccurate estimate in crack growth.

The two lower plots follow the scheme utilized in the current analysis. In this process the nodal stress data from the bottom of the nozzle to an elevation just above the bottom of the J-weld is selected. In this manner the stress distribution in the region of interest is chosen for the regressed curve fitting. This is necessary since the stresses in the weld region show significant variation (top plot) and cannot be adequately represented by a third-order polynomial. Limiting the stress distribution data to the region of interest would limit the variation and results in a more accurate fit. The plots in the lowest row, in Figure 26, show the improvement in the accuracy of fitting. The regression fit does provide an accurate representation of the stress distribution of the region. Therefore, the stress distribution used in the fracture mechanics analysis would be a reasonably accurate representation of the actual stress distribution in the region where the initial crack and subsequent crack growth are of interest.

This example and the associated plots in Figure 26 show that the regression method, as developed for the current analyses, provides an adequate representation of the stress distribution.

The analysis worksheets (Appendix C) contain a cautionary statement such that inaccurate regression is avoided. The Mathcad worksheet used to develop this example is presented in Appendix D, Attachment 1. However, it should be

noted that this attachment is not annotated but does follow the method used in the analysis worksheets.
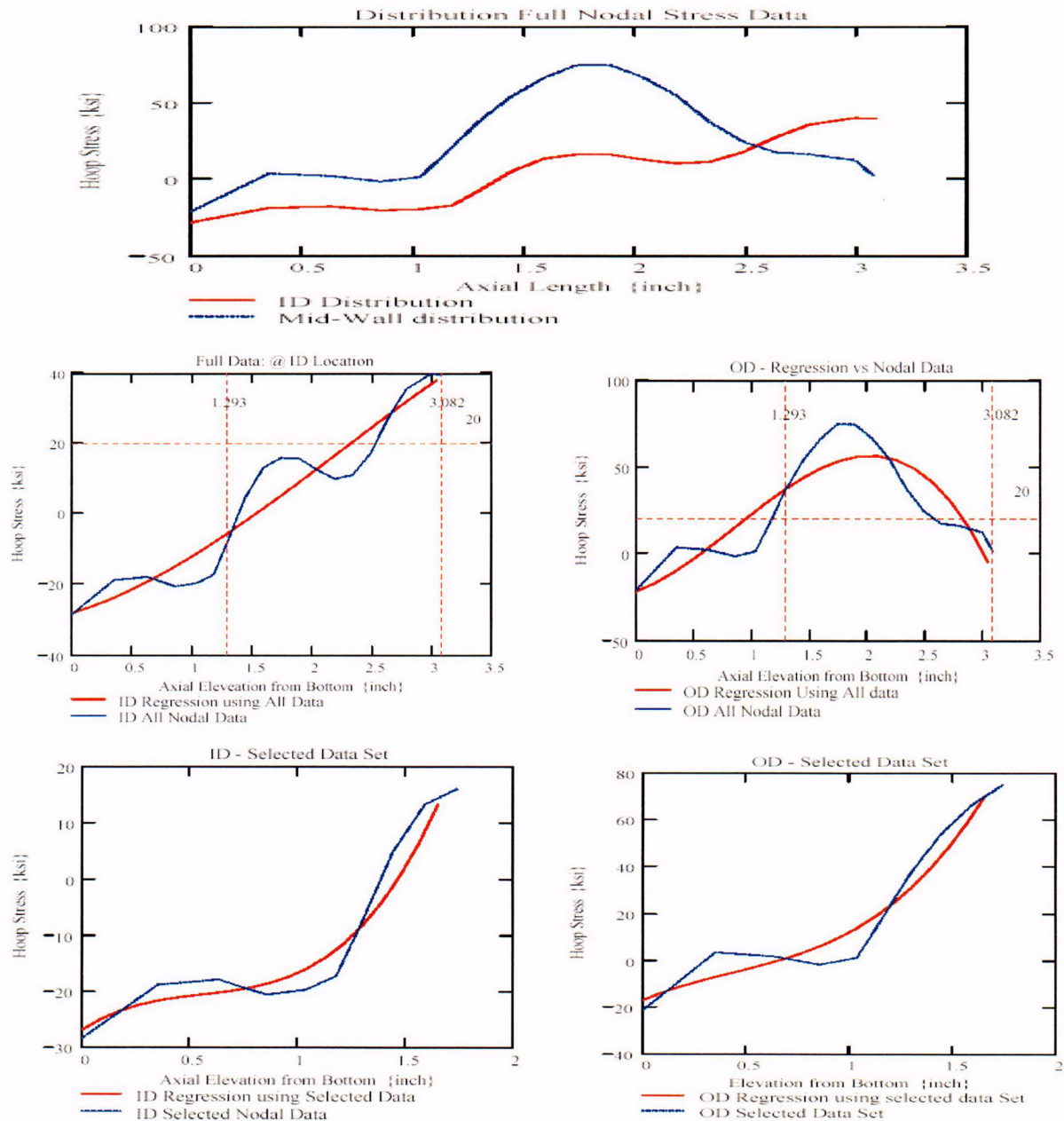
Figure 26: *Plots showing effect of nodal data selection on the accuracy of polynomial regression fit. The first plot represents all nodal stress data from the nozzle bottom to the top of the J-weld.*

The two plots, in the middle row, are the comparison of regression fit with nodal stress data; the full data set of nodal data for the ID and OD distribution was used.

The two plots, in the lower row, use a limited data set comprising the axial length to the bottom of the weld. The regression curve shows a significantly improved fit to the data.

CZZ

Once the five polynomial equations for the axial distribution are established, the through-wall stress distribution for the three locations defined by the crack and the twenty segments are established. The distributions at the twenty-three locations are subjected to a third order polynomial regression to obtain the coefficients describing the through-wall distributions. These coefficients are used within the recursive loop to assign the coefficients based on the current crack location. The five axial distributions are used for the surface cracks (ID and OD) whereas only two are required for the through-wall crack (ID and OD distributions).

Iterative Analysis to Determine SICF

For the surface cracks (ID and OD) the SICF coefficients were incorporated in two data tables. The first table contains the geometry data (R_m/t, a/c and a/t) and the second table consists of the SICF data for the appropriate cylinder and crack geometry. The values for the data were obtained from Reference 7. The data contained in the two tables were regressed into function statements with an appropriate polynomial order. The data for cylinder geometries from R_m/t ranging from one (1) to four (4) were regressed with a third-order polynomial, and for those above four, a second-order polynomial was used. The selection of the polynomial order was based on matching the value in the table given, for a selected set of independent variables, with that obtained from the interpolation performed using the regressed coefficients. In this manner the accuracy of the regression-interpolation method was established. The interpolation equation was defined outside the recursive loop and function call was made inside the loop using the pertinent variables at the time of the call.

The through-wall crack SICF was obtained using the fifth-order polynomial equation presented earlier. These equations were provided inside of the recursive loop.

The recursive loop starts the calculation scheme to determine the crack growth for a specified time period under the prevailing conditions of applied stress. The first few statements are the initialization parameters. The calculation algorithm begins with the assignment of the through-wall stress coefficients based on the current crack location. Once the four coefficients (uniform, linear, quadratic and cubic) are assigned, the through-wall stress distribution is used as the basis to establish the stress distribution along the crack face in the crack depth direction. That is , the stresses through the thickness are used to determine the stress along the crack face for application in the determination of the SIF in accordance with Reference 7. Once again, five locations along the crack depth were used to define the crack face distribution. The stresses representing the crack face values were regressed with a third-order polynomial to obtain the stress coefficients that would be used in the determination. At this point, the internal pressure is added to the stress coefficient (SCIF) for the uniform term. Therefore, the crack face is subjected to an additional stress representing the internal pressure.

Following the determination of the stress coefficients, the function call to obtain the four SICF coefficients is made. In this case the two function calls were necessary to account for the "a-tip" and the "c-tip". The crack shape factor ("Q") was then computed using the appropriate crack dimensions. The SIF is calculated separately for the "a-tip" and the "c-tip" using the stress coefficients, appropriate SICFs and crack dimensions.

In the through-wall crack solution; the fifth-order polynomial equations were solved using the current crack dimensions. The SIFs were computed for both the ID and OD locations and were then averaged. This averaged SIF was used for crack growth calculation. The crack growth calculation and the remainder of the program for both the surface cracks (ID and OD) and through-wall crack are identical.

The calculated SIFs were converted to metric unit for the computation of crack growth. The crack growth rate, based on the prevailing SIF was computed in metric units. Once this was done, a conditional branch statement was used to calculate the crack growth within the prescribed time increment. The crack growth was computed in English units by converting the calculated crack growth rate in meters-per-second to inches-per-hour. Thus, the crack growth extent was obtained in inches for the specified time period. Since the operating time was selected to be four years and the number of iterations chosen at one thousand five hundred (1500), the time increment for each crack growth block was about twenty-four (24) hours. After the calculations were performed, all necessary information (crack growth, SIFs etc.) was assigned to an output variable such that it is stored in an array. The last step of the recursive loop consisted of updating the essential parameters (namely, the index, crack length, time increment etc.).

Graphical displays of the results using both Mathcad and Axum plots complete the work sheet. The Mathcad plots are used to determine whether or not the crack reached the bottom of the weld in one operating fuel cycle and the Axum plots were generated for incorporation into this report.

The three attachments in Appendix B are sufficiently annotated to provide summary details for each major step in the program.

5.0 Discussion and Results

Discussion

The goal of the inspection program designed for the reactor vessel head penetrations is to ensure that the postulated crack in the vicinity of the blind zone does not reach the weld during the upcoming operating cycle following the refueling outage when the inspections are performed. Safety analyses performed by the MRP have demonstrated that axial cracks in the nozzle tube material do not pose a challenge to the structural integrity of the nozzle. Axial cracks, if allowed to exist undetected for sufficient periods of time can produce a primary boundary leak that can cause damage to the reactor vessel head (carbon steel) and create a conducive environment for initiating and propagating OD circumferential cracks. These conditions challenge

the pressure boundary; hence, critical importance is paid to proper periodic inspection and to the disposition of cracks that may be discovered. Therefore, proper analyses are essential to ascertain the nature of axial crack growth such that appropriate determination can be accomplished.

The analyses performed in this report were designed to capture the behavior of postulated cracks that might exist in the blind zone for the CEDM nozzle. The growth region for the postulated cracks was to the bottom of the weld along the tube OD.

The design review of the reactor vessel head construction, the detailed residual stress analyses, the selection of representative nozzle locations, selection of representative fracture mechanics models, and the application of a suitable crack growth law has provided the bases for arriving at a comprehensive and prudent decision.

The axial crack geometry is selected for evaluation because this crack has the potential for propagation into the pressure boundary weld (the J-groove weld); and since the circumferentially oriented cracks will not propagate towards the pressure boundary weld, this crack type is not evaluated. The hoop stress distribution at the downhill location (0°), at the Mid-Plane location (90° rotated from the downhill), and at the uphill (180°) location were chosen for evaluation. The axial distribution of the hoop stress magnitude for both the ID and OD surfaces shows that at axial location below the evaluated elevation, the stresses drop off significantly and become compressive except for the mid-plane location on the 49.6° nozzle group where the ID stays in tension; hence, the potential for PWSCC crack growth would be significantly low to non-existent in these locations.

The fracture mechanics evaluation considered the crack face to be subjected to the operating reactor coolant system (RCS) pressure. This is accomplished by arithmetically adding the RCS pressure to the uniform stress coefficient in the surface crack analysis and to the membrane stress for the through-wall crack analysis. In this manner, the stress imposed on the crack is accurately and conservatively modeled.

In order to ensure that the moving average technique did not create numerical errors, a Mathcad worksheet was created by using the stress averaging portion of the regular analysis worksheet. In this worksheet, the data table, which is used to import data from an Excel spreadsheet, was entirely populated with a linear through-wall stress distribution. The axial distribution of the stresses along the axis was kept constant. In this manner, the moving average method should provide results that have the same distribution at all locations along the tube axis. This implies the through-wall distribution is invariant along the length of the tube. The example and the associated worksheet are provided in Appendix D, Attachment 2. The results of the experiment show that the stress distribution across the wall remained unchanged along the axis of the tube. Therefore the moving stress averaging method is validated.

The through-wall axial crack could have been considered as a single edge crack in a plate. For this model to work properly, it is essential that the plate geometry be described accurately. The CEDM nozzle is welded to the head; hence the nozzle OD surface is clamped at the bottom of the weld. Therefore, the plate height would be equal to the length of the nozzle from the bottom of the nozzle to the bottom of the J-weld. When this plate height is assumed and the length of the through-wall axial crack is taken to be the length (height) of the blind zone, then the ratio of crack length to the plate height (assumed) violates the pre-requisite for the SICF of 0.6. It is possible to assume the plate height to be equal to the nozzle height or some smaller elevation (e.g. length equal to top of the J-weld). These assumptions tend to keep the crack-to-plate height ratio within the limit; however, the resulting SICF is lower than the membrane SICF from the model used in this analysis. A Mathcad worksheet showing the comparison is presented in Appendix D, Attachment 3. The results presented in this attachment demonstrate that the SICF for the model used in the current analysis is higher than the SICF produced by an edge crack model with longer plate lengths. In addition, the bottom zone of the CEDM nozzle is in compression, as shown in Figures 8-23, which further argues against postulating an edge crack for evaluating a through-wall crack. Therefore, for the two reasons cited herein the model developed for through-wall crack is considered valid and provides an accurate (but conservative) estimate of the SIF. The SICF comparison is presented in Figure 27 below.
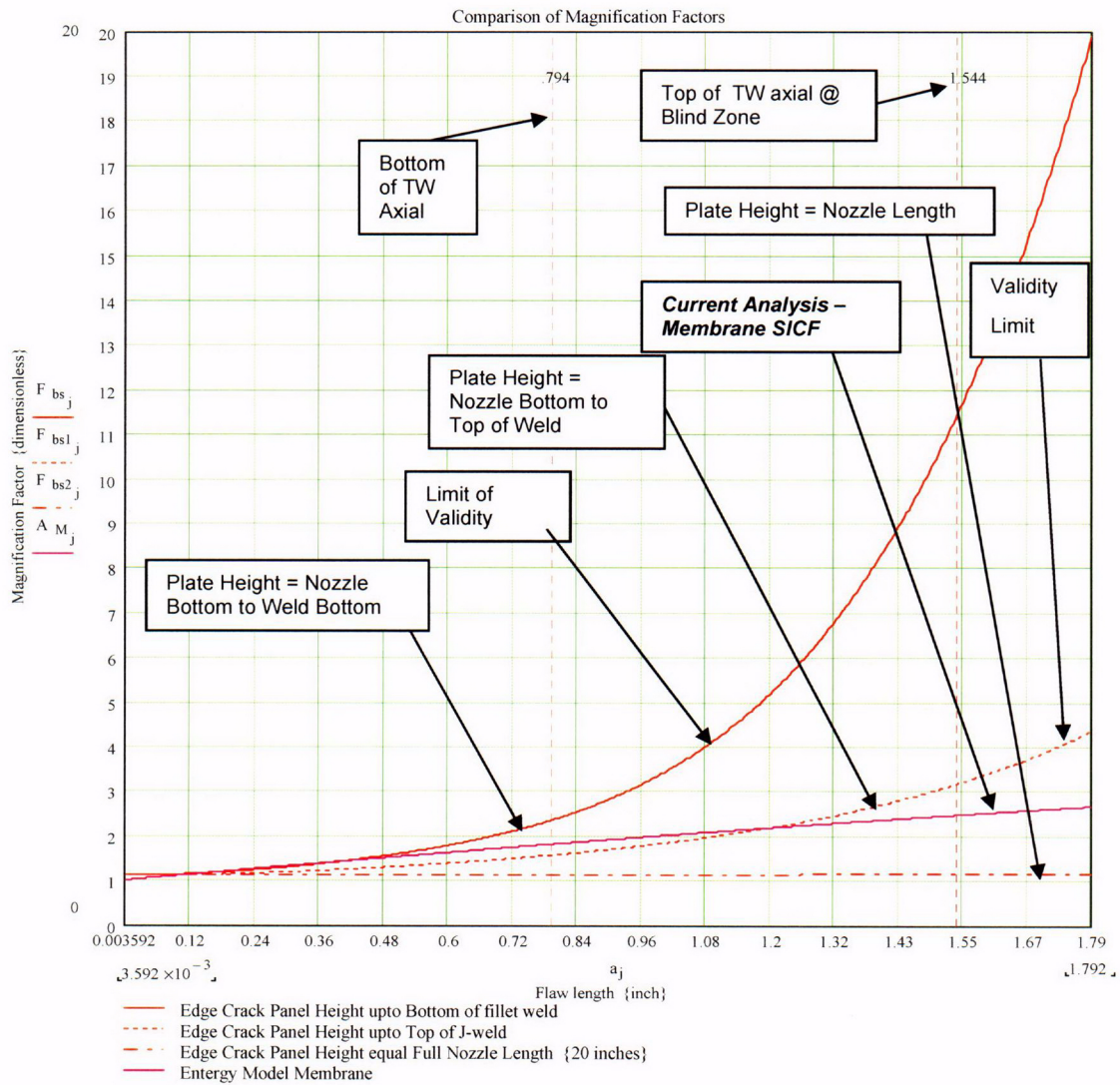
Figure 27: *Comparison of SICF for the edge crack configurations with the membrane SICF for current model. The current model results in a higher SICF value for the application considered.*

The models used in the analysis presented here were compared with the conventional approach used by the industry. The OD surface crack evaluated shows that the model used provides a higher SIF and, in addition, has the capability of separately evaluating the SIF at the two crack locations (the "a-tip" and the "c-tip"). The SIF comparison for a sample case from Appendix D, Attachment 4 is shown in Figure 28.
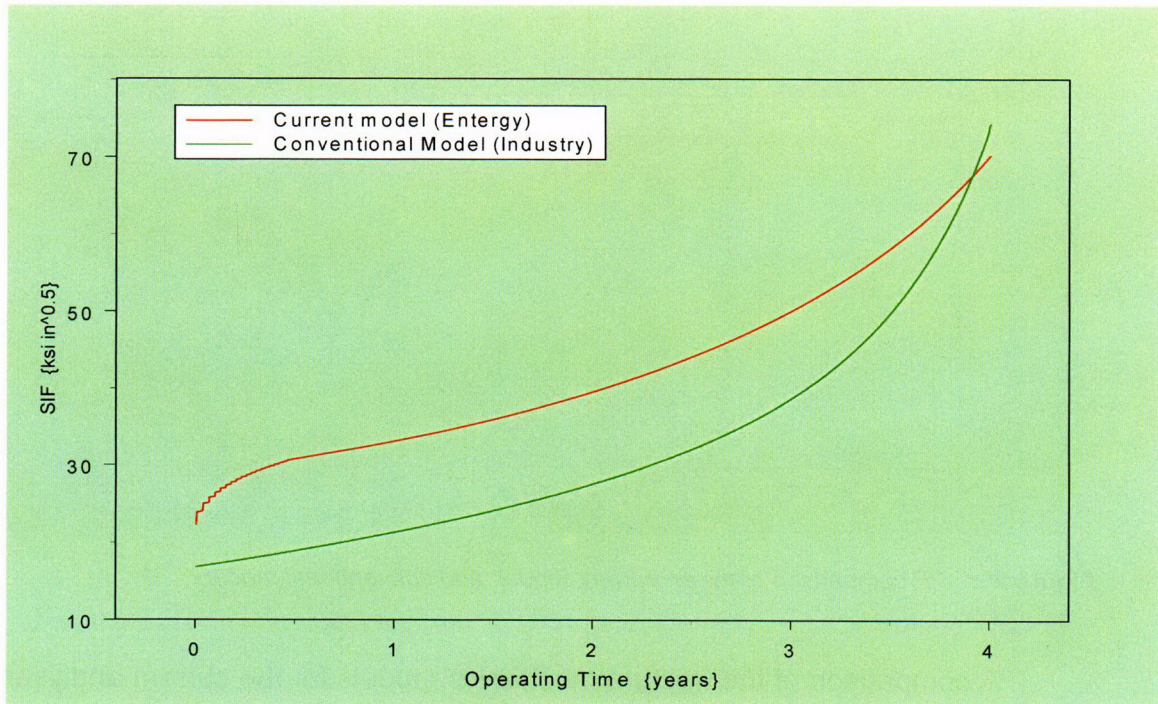
Figure 28: *Comparison of SIF for the current model and conventional model.*

The conventional approach for the through-wall axial crack is the Center Cracked Panel (CCP) with an SICF of one (SICF = 1.0). This conventional model is compared to the current model used within this analysis. The Mathcad worksheet for this comparison is presented in Appendix D, Attachment 5. The results presented in this attachment clearly demonstrate that the SIF obtained by the current model is significantly higher than that from the conventional approach. Therefore, the estimated crack growth would be higher for the current model than that estimated using the conventional approach. This would lead to an underestimate of the crack growth, by the conventional model, leading to a non-conservative propagation length estimate. Figure 29 shows a comparison between the conventional and current models.

C24
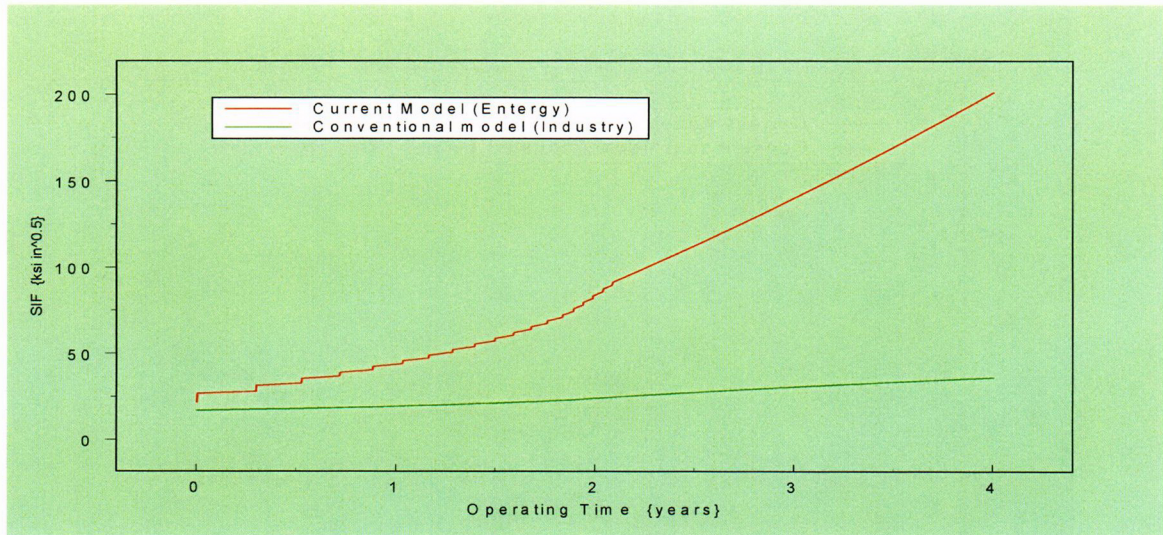
Figure 29: *SIF comparison between current model and conventional model.*

A comparison of the fracture mechanics models for the current analyses and the conventional method are summarized in Table 17. The comparison shows that the models used in the current analyses would provide a higher estimate for the SIF. The net result would be a higher crack growth rate and hence a larger crack propagation length for one (1) cycle of operation. These improvements in analysis methods are believed to more accurately predict crack behavior in the CEDM configuration and may be conservative compared to the conventional approach.

Table 17 Comparison of Fracture Mechanics Models

Flaw Type	Feature	Conventional Approach	Entergy Approach
Surface Flaws (ID & OD) Part Throughwall	Stress	Distribution Fixed a Initial flaw Location	Variable Distribution along Length of Tube & Flaw face Pressurized
	Cylinder Geometry	Fixed "R/t" ratio of 4.0	Variable "R/t" ratio from 1 to 300
	Flaw Geometry	Fixed Aspect Ratio; "a/c" = 0.33	Variable Aspect Ratio; "a/c" from 0.2 to 1.0
	Flaw Growth	Only Growth in Depth direction Evaluated	Growth both in the Depth and Length directions evaluated Independently
Throughwall Axial Flaws	Stress	Uniform Tension @ Initial flaw Location	Variable along Length; Both Membrane and Bending components considered; Flaw face Pressurized
	Model	Center Cracked Panel without Correction Factors	Thick Cylinder with correction for Flaw/Tube geometry

C25

Results

Analysis for the As-Built Condition

The first set of analyses was performed using the as-built dimensions for the welds which were estimated from the review of UT data. In addition, these analyses were performed by setting the blind zone elevation at 1.544 inches above the nozzle bottom. These analyses were performed at three azimuthal locations on the nozzle (downhill, mid-plane, and uphill). At each location, three crack geometries (ID surface, OD surface, and through-wall) were evaluated. The extent of the compression zone in each nozzle group at the three locations was obtained from the stress distributions presented in Figures 8-23. From these figures, the compression zone at the three azimuthal locations is presented in Table 18, below. In these regions of compression, no PWSCC-assisted crack growth is possible; therefore, these zones can be excluded from consideration for inspection.

Table 18: Results for Compression Zone

Nozzle Group (Head Angle – Degrees)	Azimuthal Location	Height of Compression Zone (inch) (Measured from Nozzle Bottom)
0	All (360°)	0.5
8.8	Downhill	0.5
8.8	Mid-Plane	0.6
8.8	Uphill	0.68
28.8	Downhill	0.8
28.8	Mid-Plane	0.81
28.8	Uphill	1.55
49.6	Downhill	0.8
49.6	Mid-Plane	0 (ID is in Tension)
49.6	Uphill	3.25

For nozzles 0° through and including 28.8°, the as-built nozzle and weld dimensions showed some nozzles with a measurable freespan length. For these nozzles, the representing nozzle groups (0°, 8.8°, and 28.8°) were evaluated for both part through-wall cracks and the through-wall crack. For the nozzles beyond 28.8°, the UT data indicates that on the downhill side of the nozzle that the weld extends to or into the blind zone. Therefore, the downhill side of nozzle group 49.6° has been excluded from the OD surface and through-wall crack analysis and has been addressed in the "Additional Analysis" portion of this report.

Twenty eight (28) analyses cases were performed. The worksheets representing these evaluations are presented in Appendix C, Attachments 1 - 28. The

results from this set of analyses are summarized in Table 19. Table 19 provides the "Propagation Dimension" which represents the available freespan for the limiting nozzle within the specific nozzle group. For the OD Crack Type, the length dimension excludes the 0.16 inches that was assumed for the portion of the crack that extends into the freespan. This information represents the limiting condition and is used to identify where "Additional Analysis" is needed to determine augmented surface examination requirements.

Table 19 also provides "Growth/Cycle" dimensions. This is the calculated crack growth for one cycle of operation and is used to evaluate the available freespan of each individual nozzle (as determined from the UT data). This is done by comparing the available nozzle freespan to the "Growth/Cycle" dimension. Where the freespan is larger, adequate margin for flaw growth is available without compromising the weld. When comparing the OD surface crack, 0.16 inch is subtracted from the available freespan to account for the portion of the assumed crack that extends into the freespan.

The analysis results indicate that one or more nozzles from each nozzle group does not possess sufficient free span to facilitate one cycle of crack growth. As evidenced in Table 18, it is either the OD part through-wall crack or through-wall crack that limits the nozzle group. In all cases evaluated, the ID part through-wall crack provides acceptable results for one cycle of operation. None of the postulated ID part through-wall cracks came close to reaching the bottom of the weld or penetrating through the wall to meet the weld. There is no evidence to support that an ID initiated part through-wall crack would provide a leak path or reach the weld within one operating cycle.

Because at least one nozzle in each nozzle group does not have sufficient freespan to accommodate crack growth and for many nozzles, the weld actually reaches to or into the blind zone, additional analysis have been performed for each nozzle group to identify the amount of area below the available freespan or below the weld when there is no freespan that is required to accommodate one cycle of crack growth.

Table 19: ANO-2 As-Built Analyses Results Summary

Nozzle Angle (Reactor Vessel Head)	Azimuth Location	Crack Type	Fracture Mechanics Analysis Results		Attachment Number in Appendix C
			Propagation Dimension (L= length; D= depth) (inch)	Growth / Cycle (inch)	
0 Degree	All	ID	0.092L/0.661D˙	.054L/.081D *	1
		OD	.092	0.101	2
		TW	0.252	0.576	3
8.8 Degree	Downhill	ID	0.082L/0.661D˙	.042L/.074D *	4
		OD	0.082	0.105	5
		TW	0.242	0.560	6
	Uphill	ID	0.682/0.661D˙	.041L/.072D *	7
		OD	0.682	0	8
		TW	0.842	0.043	9
	Mid-Plane	ID	0.383L/0.661D˙	.053L/.081D *	10
		OD	0.383	0.02	11
		TW	0.543	0.229	12
28.8 Degree	Downhill	ID	0L/0.661˙	.010L/.048D *	13
		OD	0		14
		TW	0.16	0.083	15
	Uphill	ID	2.564L/0.661D˙	0L/0D *	16
		OD	2.564	0	17
		TW	2.724	0	18
	Mid-Plane	ID	1.295L/0.661D˙	0L/0D *	19
		OD	1.295	0	20
		TW	1.455	0	21
49.6 Degree	Downhill	ID	na-L/0.661D˙	0L/0D *	22
	Uphill	ID	4.924L/0.661D˙	0L/0D *	23
		OD	4.924	0	24
		TW	5.084	0	25
	Mid-Plane	ID	2.33L/0.661D˙	0L/0D *	26
		OD	2.33	0	27
		TW	2.49	0	28

For ID Surface Cracks the dimensions for both in Length (L) and Depth (D) are provided.

The graphical presentation of results for those nozzle groups which showed insufficient propagation length are discussed below, by nozzle group. In the graph for length growth, a vertical red line represents one fuel cycle and a horizontal blue line representing available propagation length. When the curve is above the intersection point of these two lines, the analysis indicates that the postulated crack would reach the bottom of the weld in one operating cycle.

0° Nozzle

This nozzle was shown to be shorter than the design specified length. The reduction in the length negatively affected the freespan length. Therefore, there was insufficient propagation length to accommodate the expected crack growth for one fuel cycle. Figure 30 and 31 show the results for the OD surface crack and the through-wall crack, respectively.
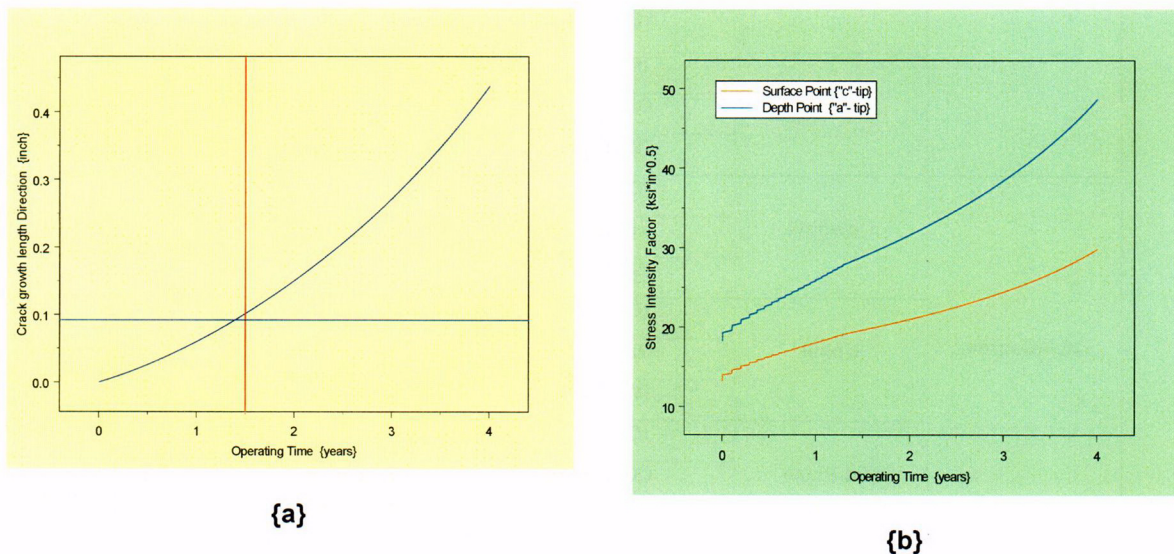

{a}

{b}

Figure 30: *Nozzle at 0°; Crack growth (a) and SIF (b) plots for an OD surface crack.*

c-26

{a}

{b}

Figure 31: *Nozzle at 0°; Crack growth (a) and SIF (b) plots for a through-wall crack.*

8.8° Nozzle Group

This nozzle was determined, based on a comparison of UT and design information, to be shorter than the design specified length. The reduction in the length negatively affected the freespan length. Therefore, there was insufficient propagation length to accommodate the expected crack growth for one operating cycle. Figures 32 and 33 show the results for the OD surface crack and the through-wall crack, respectively.

{a}

{b}

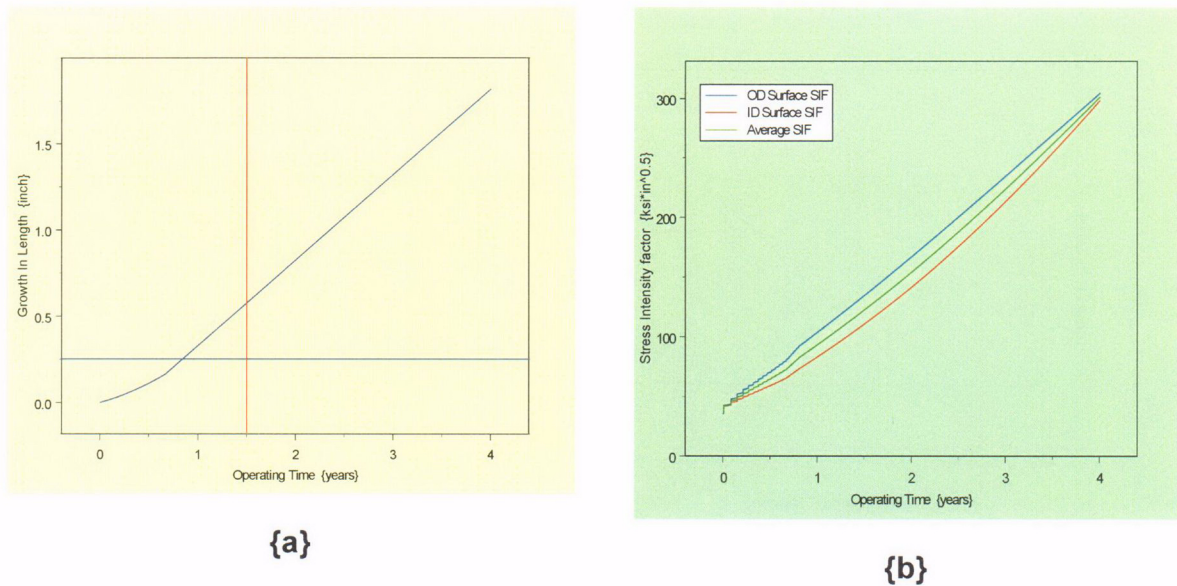**Figure 32:** *Nozzle at 8.8°; Crack growth (a) and SIF (b) plots for an OD surface crack*

C27

{a}   {b}

Figure 33: *Nozzle at 8.8°; Crack growth (a) and SIF (b) plots for a through-wall crack.*

28.8° Nozzle Group

The results for this nozzle location at the downhill position showed the crack growth for the OD surface crack to be greater than the available propagation length in one operating cycle. As stated earlier the through-wall crack growth was within the available propagation length. In Figures 34 and 35 the graphical presentation for the OD surface crack and the through-wall crack are provided. A comparison of the two figures shows that the growth is marginal and is the result of the crack placement in the analysis.
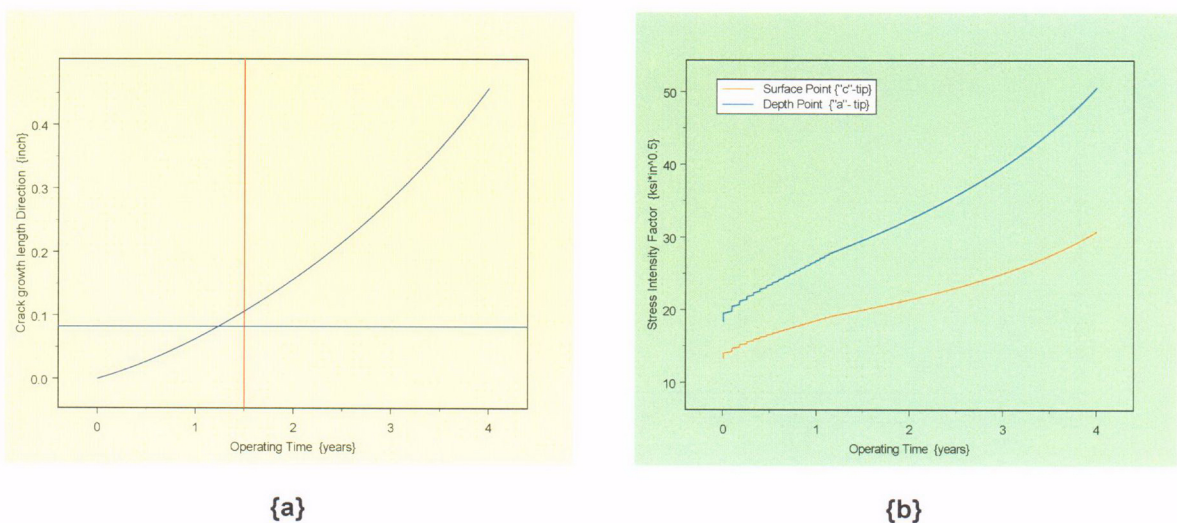

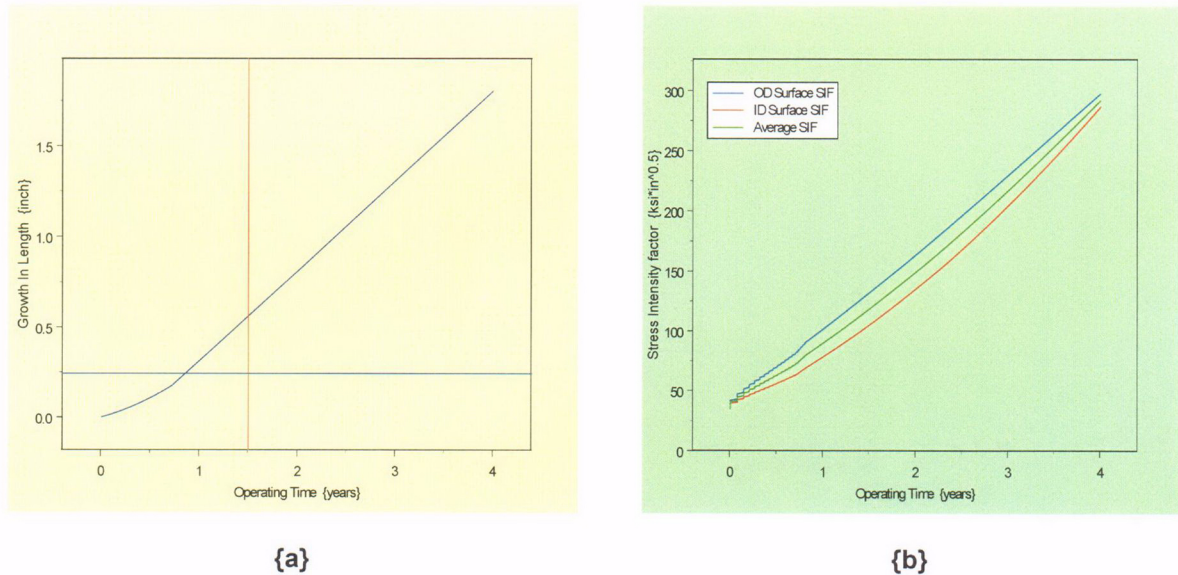{a}   {b}
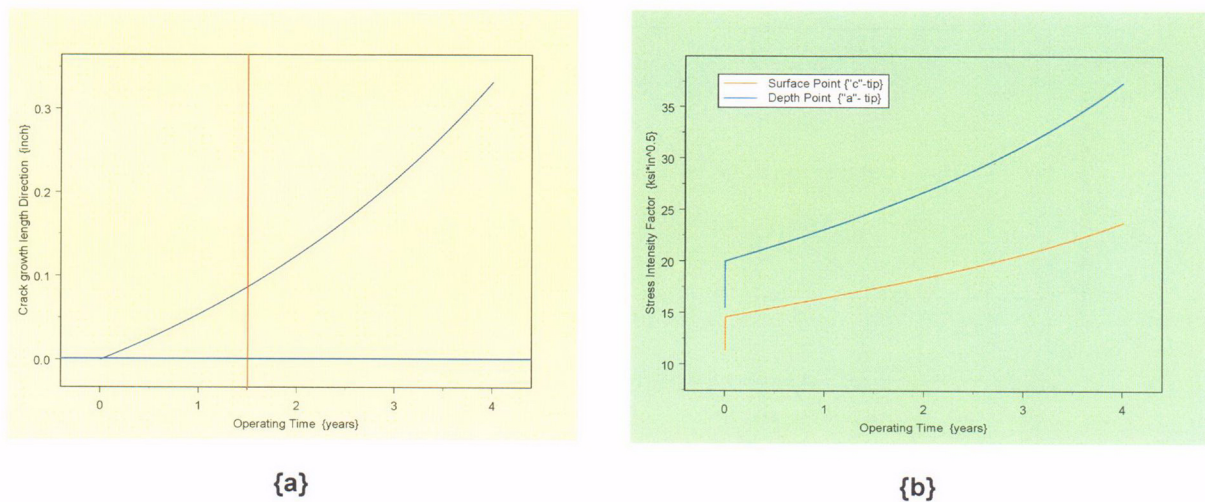
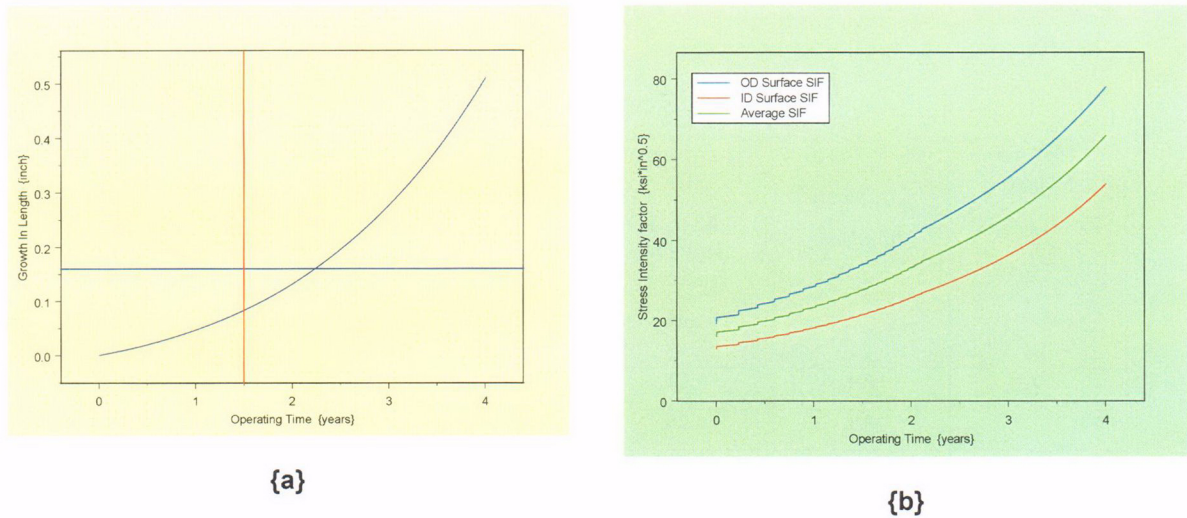**Figure 34:** *Nozzle at 28.8°; Crack growth (a) and SIF (b) plots for an OD surface crack*

{a}

{b}

Figure 35: *Nozzle at 28.8°; Crack growth (a) and SIF (b) plots for a Through-wall crack.*

Comparing Figures 34 and 35 it is observed that the through-wall crack growth does not reach the weld bottom within two years and the SIF for the two crack types are very similar (25-30 ksi√in). The marginal crack growth for both crack types coupled with the acceptable result for the through-wall crack provides reasonable assurance that for this nozzle group the OD crack result would not be controlling.

Additional Analysis

The failure to achieve acceptable crack growth for the postulated cracks in all the nozzle groups necessitated additional analysis to ascertain the augmented inspection region. Since the unacceptable condition related to the OD surface and through-wall crack types, these crack types were reevaluated to define a new region, an extended inspection area, such that acceptable crack growth for one cycle of operation was obtained. In the additional evaluations, the reference line was lowered(below the original blind zone) and the circumferential extent, around the nozzle OD circumference, was iteratively evaluated such that the original UT blind zone was recovered. In this manner the available freespan above the original blind zone and below the weld was sufficient to accommodate one (1) cycle of crack growth.

In this additional evaluation the 49.6° nozzle group at the downhill location, for OD surface and through-wall cracks were also included, since these cracks could not be evaluated using as-built conditions as the weld bottom was below the original blind zone elevation. The additional analysis for the downhill location was similar to that for the analyses process described above. Thus the augmented inspection zone for this group of nozzles was defined in a similar manner.

Results from the additional analysis performed on select nozzle groups are presented in Table 20.

Table 20: Results from Additional Analysis

Nozzle Group Head angle (Degrees)	Azimuthal Location (Degrees)	Reference Line[1] Above Nozzle Bottom (inch)	Crack Type Evaluated	Propagation Length Available (inch)	Crack Growth in One Cycle (inch)	Appendix C Attachment Number
0	All	1.25	OD	0.386	0.0275	39
	All	1.25	TW	0.546	0.2257	33
8.8	0 (downhill)	1.25	OD	.376	0.026	40
	0 (downhill)	1.25	TW	.536	0.202	34
	DH±22.5	1.3	OD	0.347	0.30	41
	DH±22.5	1.3	TW	0.507	.227	43
	DH±45	1.544	OD	0.167	0.071	42
	DH±45	1.45	TW	0.421	0.345	44
	DH±67.5	1.544	OD	0.263	0.044	46
	DH±67.5	1.544	TW	0.426	0.354	45
28.8	0 (downhill)	1.384	OD	0.16	0.0267	47
	DH±22.5	1.544	OD	0.128	0.05	31
	DH±22.5	1.544	TW	0.288	0.15	48
49.6	0 (downhill)	1.043	OD	0.09	0	29
	0 (downhill)	1.043	TW	0.25	0	30
	DH±22.5	1.3	OD	0.09	0.028	35
	DH±22.5	1.3	TW	0.25	0	37
	DH±45	1.544	OD	0.459	0	36
	DH±45	1.544	TW	0.619	0	38

1) *Input to analysis to adjust postulated crack location to identify the axial extent required for one (1) cycle of crack growth.*

The analysis results presented in the table above were obtained from specific analysis worksheets provided as Attachments 29 through 48 of Appendix C.

The blue text color in the column labeled "Reference Line" indicates the lowest location of the reference line required to provide sufficient propagation length to support one cycle of operation. The rows colored in yellow show the circumferential (azimuthal) extent required to recover the original blind zone of 1.544 inches. Thus, the two required boundaries for the candidate nozzles are obtained and the required

augmented inspection zone, for OD-based surface examination, can be defined. It is important to note that the OD surface crack's upper half-length is placed above the reference line, hence the axial elevation for the augmented inspection is reduced by the OD crack half-length (0.16 inch). Conversely the axial extent for the augmented inspection is increased by 0.16 inch. The boundaries of the augmented inspection are provided in Table 21 below. The location of the lower extent for the augmented inspection (that is the lower boundary), defined as an elevation above the nozzle bottom, was based on the necessary propagation length for the OD surface crack. Therefore, the boundary is conservative for a through-wall axial crack. Recall that the modeling for an OD surface crack assumes that the lower tip and the upper tip of the crack are placed 0.16 inch below and above the reference line respectively. In the additional analyses the reference line was located below the elevation for the top of the blind zone. The dimension for the axial boundary locations (bottom and top boundary), in Table 21, is the elevation above the nozzle bottom. Hence the full extent of the assumed surface crack is covered. Likewise, the circumferential extent forms an arc on either side of the downhill (0°) location. The included angle of the arc is twice (2) the angle dimension in Table 21. That is the reason for the sign in front of the angle number.

Table 21: Boundaries for Augmented Inspection (OD Surface Examination)

Nozzle Group	Specified Boundary for Augmented Surface Examination (OD)	
Head Angle (Degrees)	Bottom and Top Boundary for Augmented Examination (Axial Elevation from Nozzle Bottom) (inch)	Azimuthal Extent from Downhill Location (Degrees)
0	1.09 to 1.544	± 180 (full circumference)
8.8	1.09 to 1.544	± 67.5
28.8	1.224 to 1.544	±22.5
49.6	0.883 to 1.544	± 45

The discussion and graphical presentation below are categorized by nozzle group. Only graphs for crack growth are provided, because these graphs are pertinent to the discussion. The other graphs are available in the attachments provided in Appendix C.

0° Nozzle

This nozzle had insufficient freespan to accommodate one cycle of postulated crack growth. In addition, this nozzle is axi-symmetric about the nozzle axis, hence, the augmented inspection region is the full circumference of the defined region. Figure 36 presents the crack growth behavior at the lowered reference line for both the OD surface and through-wall crack geometry.
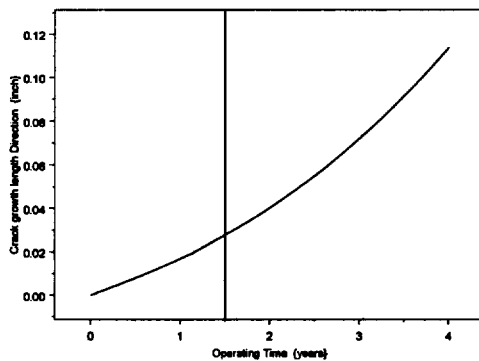
| OD Surface Crack; Propagation Length = 0.386" | Through-wall Crack |
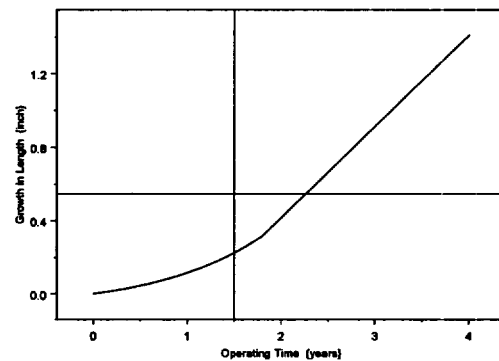
Figure 36: *0° Nozzle crack growth at lowered reference line at 1.25 inches above nozzle bottom. The augmented inspection coverage in the azimuthal direction is the full circumference.*

8.8° Nozzle Group

This nozzle group had insufficient propagation length to accommodate one cycle of postulated crack growth. The augmented inspection region in the azimuthal direction is an arc of 135° centered about the downhill location (0°). Figure 37 presents the crack growth behavior at the original blind zone at 1.544 inches above nozzle bottom and the 67.5° azimuth for both the OD surface and through-wall crack geometry.
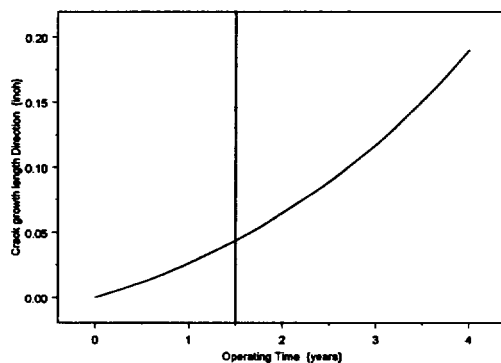
| OD Surface Crack; Propagation Length = 0.263' | Through-wall Crack |

Figure 37: *8.8° Nozzle crack growth at blind zone elevation of 1.544 inches above nozzle bottom and at an azimuth of 67.5°. The augmented inspection coverage in the azimuthal direction is a 135° arc centered at the downhill location (0°).*

28.8° Nozzle Group

This nozzle group had insufficient propagation length to accommodate one cycle of postulated crack growth for the OD surface crack. The through-wall crack had sufficient propagation length to accommodate one cycle of postulated crack growth. The augmented inspection region in the azimuthal direction is an arc of 45° centered about the downhill location (0°). Figure 38 presents the crack growth behavior at the original blind zone at 1.544 inches above nozzle bottom and the 22.5° azimuth, for both the OD surface and through-wall crack geometry.

OD Surface Crack; Propagation Length = 0.16"

Through-wall Crack

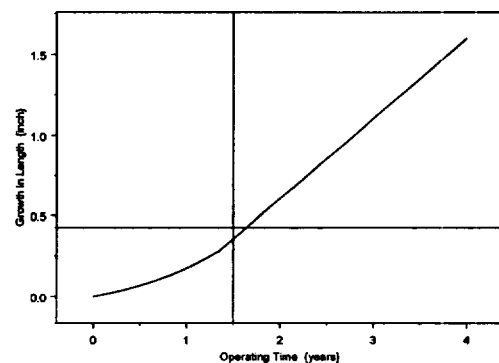**Figure 38:** *28.8° Nozzle crack growth at the blind zone elevation of 1.544 inches above nozzle bottom and at an azimuth of 22.5°. The augmented inspection coverage in the azimuthal direction is a 45° arc centered at the downhill location (0°).*

49.6° Nozzle Group

This nozzle group had the weld bottom extend into the blind zone at the downhill location. Hence, a lowered reference line was used to define the augmented inspection zone. The analysis was performed at the two different azimuthal locations to ensure the recovery of available propagation length above the original blind zone at 1.544 inches above nozzle bottom. At an azimuth of 45°, the analysis showed that there exists sufficient propagation length above the original blind zone to accommodate one cycle of postulated crack growth. The augmented inspection region in the azimuthal direction is an arc of 90° centered about the downhill location (0°). Figure 39 presents the crack growth behavior at the original blind zone and the 45° azimuth, for both the OD surface and through-wall crack geometry.

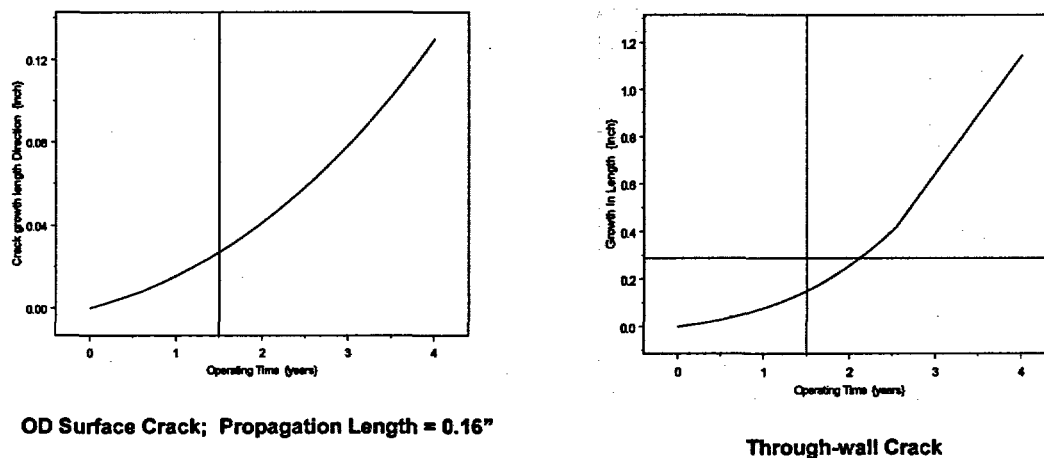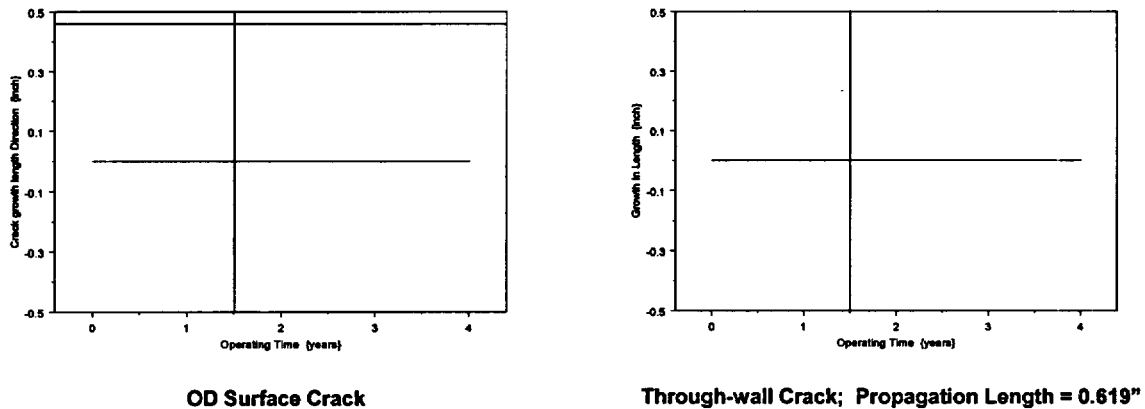OD Surface Crack   Through-wall Crack; Propagation Length = 0.619"

Figure 39: *49.6° Nozzle crack growth at the blind zone elevation of 1.544 inches above nozzle bottom and at an azimuth of 45°. The augmented inspection coverage in the azimuthal direction is a 90° arc centered at the downhill location (0°).*

6.0 Conclusions

The evaluation performed and presented in the preceding sections support the following conclusions:

1) The detailed deterministic analyses incorporating the as-built dimensions for the weld and nozzle length were used to accurately define the inspection zones for the CEDM nozzle groups.

2) The developed models, incorporating a method to account for applied stress distribution variation along the nozzle length, have been shown to be a reasonably realistic but conservative representation of the expected phenomenon. The models are generalized and have the potential to be used at other locations of the nozzles.

3) The fracture mechanics models were shown to be representative of the expected crack and nozzle configurations. A review of the current model results and that from the conventional approach showed that the current model produced higher SIF than the conventional model. Therefore, the current model provides a more accurate and conservative estimate of crack growth.

4) The conservatisms used in the analysis provide assurance that an undetected crack at the lowest elevation for inspection will not reach the weld bottom within one operating cycle.

5) The regions below the lowest inspection elevation experience lower stresses and except for the one exception noted within the report, there exists a defined compressive zone at the nozzle bottom. Hence, at elevations below the lowest inspection elevation, a significantly lower

potential for crack growth by PWSCC exists. Thus, at these lower locations PWSCC, crack growth is not expected.

6) The ID surface cracks either did not show any potential for crack growth, or the crack growth was well within acceptable limits. Hence, ID surface cracks in a region below the weld are not significant.

7) The augmented inspection region, developed by the deterministic analysis, will provide assurance that a postulated crack below the proposed inspection zone will not reach the bottom of the weld in one operating cycle.

References

1) NRC Order; Issued by letter EA-03-009 addressed to "Holders of Licenses for Operating Pressurized Water Reactors"; dated February 11, 2003.

2) Drawing Number M-2001-C2-23, ANO Design Engineering Drawing files & 1564-506 WSES-3 Design Engineering Drawing files.

3) a: E-mail from R. V. Swain (Entergy) to J. G. Weicks (Entergy); Dated 5/15/2003.

   b: E-mail from R. V. Swain to J. G. Weicks; Dated 5/12/2003.

4) EPRI NDE Demonstration Report; "MRP Inspection Demonstration Program – Wesdyne Qualification": Transmitted by e-mail from B. Rassler (EPRI) to K. C. Panther (Entergy); Dated 3/27/2003.

5) a: "PWSCC of Alloy 600 Materials in PWR Primary System Penetrations"; EPRI TR-103696; Electric Power Research Institute, Palo Alto, CA; July 1994.

   b: DEI E-Mail containing the Nodal Stress Data for ANO-2 CEDM Analysis; J. Broussard (DEI) to J. S. Brihmadesam (Entergy); Dated 8/17/2003

   c: "BWR Vessel and Internals Project – Evaluation of crack growth in BWR Stainless Steel RPV Internals (BWRVIP-14)"; EPRI TR-105873; Electric Power Research Institute, Palo Alto, CA; March 1996.

   d: "BWR Vessel and Internals Project – Evaluation of crack growth in BWR Nickel Base Austenitic Alloys in RPV Internals (BWRVIP-59)"; EPRI TR-108710; Electric Power Research Institute, Palo Alto, CA; December 1998.

6) "Stress Intensity Factor Influence Coefficients for Internal and External Surface Cracks in Cylindrical Vessels"; I. S. Raju and J. C. Newman, Jr.; ASME PVP Volume 58 "Aspects of Fracture Mechanics in Pressure Vessels and Piping"; 1982.

7) "Stress Intensity Factors for Part-Through Surface Cracks in Hollow Cylinders": S. R. Mettu etal; NASA TM-111707; Prepared by Lockheed Engineering & Science Services; Houston, Texas; July 1992.

8) "New Stress Intensity factor and Crack Opening Area Solutions for Through Wall Cracks in Pipes and cylinders": Christine C. France, etal.; ASME PVP Volume 350 "Fatigue and Fracture"; 1997.

9) Axum 7; Data Analysis Products Division, Mathsoft Inc., Seattle, WA; February 1999.

10) "Materials reliability Program (MRP) Crack Growth Rates for Evaluating Primary Water Stress Corrosion cracking (PWSCC) of Thick Wall Alloy 600 Material": MRP-55 Revision 1; Electric Power Research Institute; May 2002.

11) Mathcad – 11; Data Analysis Products Division; Mathsoft Inc.; Seattle WA; November 2002.

12) "Stress Intensity Factors Handbook Volume 1"; Y. Murakami, Editor-in-Chief; Pergamon Press ; 1986; Section 1.3.

Appendix A

This Appendix contains design information, UT analysis data and an evaluation to determine the best-estimate as-built configuration.

This Appendix has five (5) Attachments.

Design Input Sheet for Fracture Mechanics Evaluation of CEDM nozzles below the Attachment J-weld
{ANO Unit 2 and WSES Unit 3}

Item	Source	Input Used	Concurrence[1]
Length from bottom of nozzle to top of thread relief counterbore (includes 1 inch thread length plus ¼ inch thread relief counterbore)	Drawing M-2001-C2-23 revision 4 (CE drawing E-234-760-2) ANO-2 E-74170-112-01 WSES-3	1.25 inches	Site Design Engineering: ANO: Jamie GoBell _(signature) 5/8/03_ WSES3:_____
Maximum Chamfer Dimension along the axis of the nozzle, including 1/32" tolerance	Same Drawing as above	0.094 inches	Site Design Engineering. ANO: Jamie GoBell _(signature) 5/8/03_ WSES3:_____
NDE Dead Zone	Ronnie Swain's Notes of 4/23/03 attached to e-mail of 4/23/03	0.300	Site Quality Programs/NDE ANO:_____ WSES3:_____
Residual Stress Distribution	DEI calculations : C-7736-00-5 ANO-2 C-7736-00-4 WSES-3	Nodal stresses below J-weld	DEI Calculations were performed for Westinghouse under contract to Westinghouse for ANO-2 and WSES3 RVHP evaluations. Westinghouse {OEM} provided design input. Westinghouse and DEI have Appendix "B" qualified QA program and these calculations were performed under the applicable program. This provides reasonable assurance that the results are applicable.
PWSCC Crack Growth rate	EPRI-MRP 55 revision 1.	Seventy-fifth Percentile Curve	EPRI report based on information provided by all utilities and the analyses for the report was performed under EPRI QA program. The report was reviewed by Utility peer group {MRP} for correctness, completeness and applicability. The information is reasonable for use for ANO-2 and WSES-3 application.
Nozzle Dimensions {ID and OD}	Drawing M-2001-C2-23 revision 4 (CE drawing E-234-760-2) ANO-2 E-74170-112-01 WSES-3	OD = 4.05"; ID = 2.719" OD = 4.05"; ID = 2.719"	Site Design Engineering: ANO: Jamie GoBell _(signature) 5/8/03_ WSE3:_____
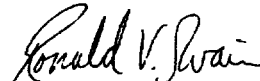
1: *Concurrence is only required for items that have a signature block. The Residual Stress results and PWSCC crack growth rate report have been provided under approved QA programs and there is reasonable assurance of the result's accuracy. Hence for these two items specific concurrence is not required.*

NDE Dead Zone Design Input

June 6, 2003

Design Input to Engineering Report M-EP-2003-002:

At the request of Entergy, Westinghouse reviewed UT data for 10 penetrations taken from the 2R15 ANO-2 reactor head inspection. This inspection was performed with a 7010 ultrasonic end-effector, using 0.250" diameter, 24mm PCS Time-of-Flight-Diffraction ultrasonic transducers. The penetrations were chosen by their location on the head, in order to provide a representative sample of the entire head. The analysis was performed in order to determine the ultrasonic dead band located immediately above the threaded region of the CEDM nozzles. This review determined the dead band to be 0.200".

Ronald V. Swain
UT Level III
Waterford 3 SES

\

To support the crack growth rate evaluation for the portion of the CEDM nozzle that extends below the J-groove weld on the ANO-2 and W-3 heads, the length of this portion of the nozzle is required. Because this length varies with the nozzle location, an Excel spreadsheet was developed to calculate the various parameters of the nozzle J-groove weld configuration.

To describe the geometry, the following nomenclature is used: The location of the nozzle relative to the curvature of the head is identified by the angle in degrees between the vertical centerline of the head, and a line created by the radius of curvature of the bottom surface of the cladding where it intersects with the centerline of the nozzle. The nozzle locations included in the crack growth rate evaluation are identified as the following:

ANO-2		Waterford-3	
Nozzle location	Penetration No.	Nozzle location	Penetration No.
0°	1	0°	1
8.8°	2, 3, 4, 5	7.8°	2, 3
28.8°	30, 31, 32, 33, 34, 35, 36, 37	29.1°	36, 37, 38, 39, 40, 41, 42, 43
49.6°	70, 71, 72, 73, 74, 75, 76, 77, 78, 79, 80, 81	49.7°	88, 89, 90, 91

The point location around the OD of the nozzle is identified by the azimuth angle with the zero degree azimuth location being the point furthest from the vertical centerline of the head, which is also the lowest point that the J-groove weld attaches to the nozzle (the "low-hillside"). The length of the portion of the nozzle that extends down below the J-groove weld is calculated at the zero degree azimuth for each of the nozzle locations evaluated.

The length, "L", of the portion of the nozzle that extends down below the J-groove weld is defined as the vertical distance from the point where the surface of the cladding would intersect with the outside surface of the nozzle at the zero degree azimuth location down to the bottom of the nozzle (see attached sketch).

Using ANO drawings M-2001-C2-23, M-2001-C2-26, M-2001-C2-32, M-2001-C2-55, and M-2001-C2-107, and Waterford drawings 1564-506, 1564-1036, and 1564-4086, the length "L" was calculated as shown in the following table:

ANO-2		Waterford-3	
Nozzle location	L (inches)	Nozzle location	L (inches)
0°	2.50	0°	2.88
8.8°	2.49	7.8°	2.88
28.8°	2.48	29.1°	2.86
49.6°	2.48	49.7°	2.92

Verified by:

ANO-2			Waterford-3		
Jamie GoBell		6/4/03	*Nara Ray*		6/4/03
Jamie GoBell		Date	Nara Ray		Date
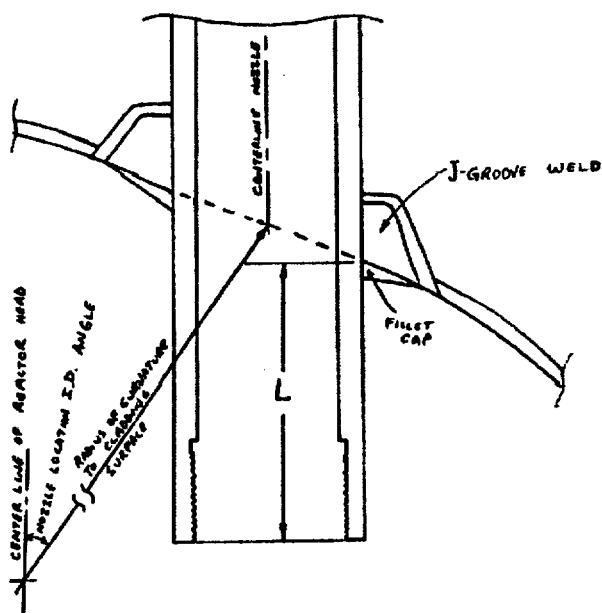
ANO-2 UT Data Measurements

**UT data obtained during last Refueling Outage
(April 2002)
Data from review of Zero degree UT Scan**

CEDM Dimensions taken from the 0 degree UT data on the ANO-2 RPV Head

OZZLE # eld		Dead Zone to Bottom of Fillet	Dead Zone to Top of J-
1		0.32"	1.24"

On nozzle #1, the dead zone is not visible on this data, so the accuracy of these dimensions are questionable.

2	Low HS	0.24"	1.20"
	High HS	0.84"	1.84"
3	Low HS	0.16"	1.24"
	High HS	0.92"	1.88"
4	Low HS	0.18"	1.24"
	High HS	0.80"	1.92"
5	Low HS	0.32"	1.24"
	High HS	1.00"	1.96"
6	Low HS	0.44"	1.40"
	High HS	1.32"	2.36"
7	Low HS	0.32"	1.52"
	High HS	1.24"	2.36"
8	Low HS	0.20"	1.44"
	High HS	1.12"	2.28"
9	Low HS	0.48"	1.52"
	High HS	1.44"	2.48"
10	Low HS	0.12"	1.60"
	High HS	1.68"	2.68"

On nozzle #10, the dead zone is not visible on this data, so the accuracy of these dimensions are questionable.

11	Low HS	0.16"	1.52"
	High HS	1.64"	2.76"
12	Low HS	0.16"	1.36"

	High HS	1.52"	2.80"

On nozzle #12, the dead zone is not visible on this data, so the accuracy of these dimensions are questionable.

13	Low HS	0.16"	1.56"
	High HS	1.68"	2.80"

On nozzle #13, the dead zone is not visible on this data, so the accuracy of these dimensions are questionable.

14	Low HS	0.0"	1.08"
	High HS	1.40"	2.48"

On nozzle #14, the dead zone is not visible on this data, so the accuracy of these dimensions are questionable.

15	Low HS	0.16"	1.60"
	High HS	1.92"	3.08"

16	Low HS	0.12"	1.44"
	High HS	1.84"	3.04"

17	Low HS	0.08"	1.44"
	High HS	1.80"	3.04"

18	Low HS	0.24"	1.48"
	High HS	1.76"	3.08"

19	Low HS	0.16"	1.52"
	High HS	1.76"	3.16"

20	Low HS	0.48"	1.52"
	High HS	1.88"	3.08"

21	Low HS	0.24"	1.44"
	High HS	1.92"	2.92"

On nozzle #21, the dead zone is not visible on this data, so the accuracy of these dimensions are questionable.

22	Low HS	0.12"	1.48"
	High HS	2.32"	3.56"

23	Low HS	0.0"	1.32"
	High HS	2.36"	3.56"

24	Low HS	0.12"	1.32"
	High HS	2.28"	3.32"

25	Low HS	0.28"	1.56"
	High HS	2.44"	3.60"
26	Low HS	0.08"	1.36"
	High HS	2.44"	3.56"
27	Low HS	0.0"	1.72"
	High HS	2.52"	3.64"
28	Low HS	0.24"	1.48"
	High HS	2.36"	3.76"
29	Low HS	0.16"	1.60"
	High HS	2.56"	3.84"
30	Low HS	0.16"	1.36"
	High HS	2.48"	3.76"
31	Low HS	0.20"	1.32"
	High HS	2.56"	3.56"
32	Low HS	0.16"	1.24"
	High HS	2.60"	3.64"
33	Low HS	0.0"	1.40"
	High HS	2.24"	3.72"
34	Low HS	0.20"	1.08"
	High HS	2.12"	3.68"
35	Low HS	0.16"	1.40"
	High HS	2.76"	3.88"
36	Low HS	0.04"	1.60"
	High HS	2.48"	3.80"
37	Low HS	0.24"	1.52"
	High HS	2.68"	4.00"
	No A-Scan data present for nozzle #37		
38	Low HS	0.0"	1.20"
	High HS	3.16"	4.32"
39	Low HS	0.0"	1.08"
	High HS	2.68"	4.16"

40	Low HS	0.0"	1.04"
	High HS	2.60"	4.04"
41	Low HS	0.0"	1.00"
	High HS	2.84"	4.24"
42	Low HS	0.0"	1.08"
	High HS	2.72"	4.04"
43	Low HS	0.0"	1.36"
	High HS	?? (probe lift-off)	4.28"
44	Low HS	0.08"	1.32"
	High HS	3.20"	4.40"
45	Low HS	0.0"	1.12"
	High HS	3.00"	4.24"
46	Low HS	0.0"	1.08"
	High HS	2.92"	4.40"
47	Low HS	0.0"	1.04"
	High HS	3.16"	4.28"
48	CD BLANK/ NO DATA AVAILABLE		
49	CD BLANK/ NO DATA AVAILABLE		
50	CD BLANK/ NO DATA AVAILABLE		
51	Low HS	0.0"	1.04"
	High HS	2.96"	4.56"
52	Low HS	0.0"	1.16"
	High HS	3.40"	4.60"
53	FAULTY CD/ NO DATA AVAILABLE		
54	Low HS	0.0"	1.04"
	High HS	3.16"	4.64"
55	Low HS	0.0"	1.12"
	High HS	3.28"	4.72"
56	Low HS	0.0"	1.40"
	High HS	3.36"	4.76"
57	Low HS	0.0"	1.16"

	High HS	3.28"	4.64"
58	Low HS	0.16"	1.12"
	High HS	3.60"	4.88"
59	Low HS	0.08"	1.12"
	High HS	3.44"	4.68"
60	Low HS	0.08"	0.96"
	High HS	3.40"	4.64"
61	Low HS	0.0"	1.28"
	High HS	3.64"	4.92"
62	Low HS	0.0"	1.00"
	High HS	3.84"	5.12"

On nozzle #62, the dead zone is not visible on this data, so the accuracy of these dimensions are questionable

63	Low HS	0.04"	1.16"
	High HS	3.76"	5.08"
64	Low HS	0.04"	0.96"
	High HS	?? (probe lift-off)	5.08"
65	Low HS	0.0"	1.00"
	High HS	3.76"	4.96"
66	Low HS	0.0"	1.00"
	High HS	3.72"	4.88"
67	Low HS	0.08"	1.56"
	High HS	3.92"	5.44"
68	Low HS	0.0"	1.52"
	High HS	3.84"	5.32"
69	Low HS	0.0"	1.36"
	High HS	3.88"	5.20"
70	Low HS	0.0"	1.44"
	High HS	5.04"	6.52"
71	Low HS	0.0"	1.32"
	High HS	5.04"	6.52"

72	Low HS	0.0"	1.32"
	High HS	5.08"	6.52"
73	Low HS	0.0"	1.20"
	High HS	5.00"	6.44"
74	Low HS	0"	1.12" 1.88"
	High HS	5.12"	6.28"
75	Low HS	0"	1.20"
	High HS	5.00"	6.40"
76	Low HS	0.0"	1.60"
	High HS	4.64"	6.52"
77	Low HS	0.0"	1.52"
	High HS	5.20"	6.44"

On nozzle #77, the dead zone is not visible on this data, so the accuracy of these dimensions are questionable

78	Low HS	0.0"	1.48"
	High HS	5.16"	6.68"
79	Low HS	0.0"	1.64"
	High HS	4.96"	6.52"
80	Low HS	0.0"	1.44"
	High HS	4.96"	6.52"
81	Low HS	0"	1.56"
	High HS	5.08"	6.48"

Analysis of UT information and Information from Design Drawings

1) Comparison of Freespan length to develop as-built nozzle configuration for Finite Element Model.
2) Development of nozzle dimension and fillet weld profile.

Analysis sequence:

1) Using design drawing information and blind zone elevation of 1.544 inch, determine design based freespan length.
2) Compare the as-designed freespan length with UT measured freespan length at both the downhill and uphill locations.
3) Record the differences.
4) Based on an evaluation of the differences, develop nozzle dimension and expected fillet weld profile.
5) Develop nozzle configuration for FEA model.

Design Analysis Information

0° Nozzle

As Designed Length	All HS	1.21	Bottom	0.56	Top	1.77

8.8° Nozzle

As Designed Bottom	Low HS	0.54
	High HS	1.17
As Designed Top	Low HS	1.73
	High HS	2.41
As Designed Length	Low HS	1.19
	High HS	1.24

28.8° Nozzle

As Designed Bottom	Low HS	0.44
	High HS	2.69
As Designed Top	Low HS	1.64
	High HS	4.09
As Designed Length	Low HS	1.19
	High HS	1.40

49.6° Nozzle

As Designed Bottom	Low HS	0.21
	High HS	5.05
As Designed Top	Low HS	1.51
	High HS	6.75
As Designed Length	Low HS	1.30
	High HS	1.71

Comparison of UT and design Data

0.0° Nozzle		Bottom		Top		Length	
		Measured	Diff	Measured	Diff	Measured	Diff
Nozzle 1	All HS	0.32	-0.24	1.24	-0.53	0.92	-0.29

8.8° Nozzle		Bottom		Top		Length	
		Measured	Diff	Measured	Diff	Measured	Diff
Nozzle 2	Low HS	0.24	-0.30	1.20	-0.53	0.96	-0.23
	High HS	0.84	-0.33	1.84	-0.57	1.00	-0.24
Nozzle 3	Low HS	0.16	-0.38	1.24	-0.49	1.08	-0.11
	High HS	0.92	-0.25	1.88	-0.53	0.96	-0.28
Nozzle 4	Low HS	0.18	-0.36	1.24	-0.49	1.06	-0.13
	High HS	0.80	-0.37	1.92	-0.49	1.12	-0.12
Nozzle 5	Low HS	0.32	-0.22	1.24	-0.49	0.92	-0.27
	High HS	1.00	-0.17	1.96	-0.45	0.96	-0.28

1) Note the differences between the bottom and top locations (Diff Column); They are consistent but the differences are 0.33 inch at bottom (both downhill & uphill) and 0.53 inch at the top (both downhill & uphill). This indicates that the nozzle may be shorter.
2) The average between the differences is about 0.4 inch, hence a nozzle that is shorter by 0.4 inches would minimize the differences between the as-designed and UT measurements.
3) The measurement for weld length (diff. in Length column) is small and random; indicating that the weld profile is close to the as-designed condition.
4) A nozzle configuration with a shorter (2.08 inches vs. 2.48 inches) by 0.4 inch with an as-designed weld profile provides the best estimate for the as-built configuration of these two nozzle groups.

Evaluation of the 28.8° Nozzle Group:

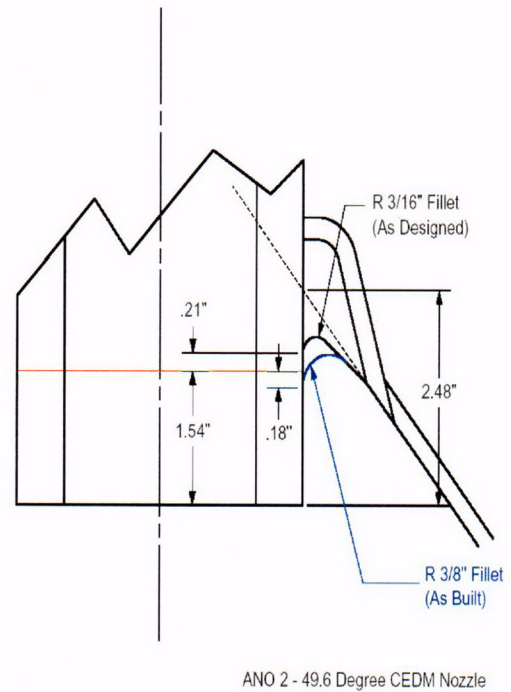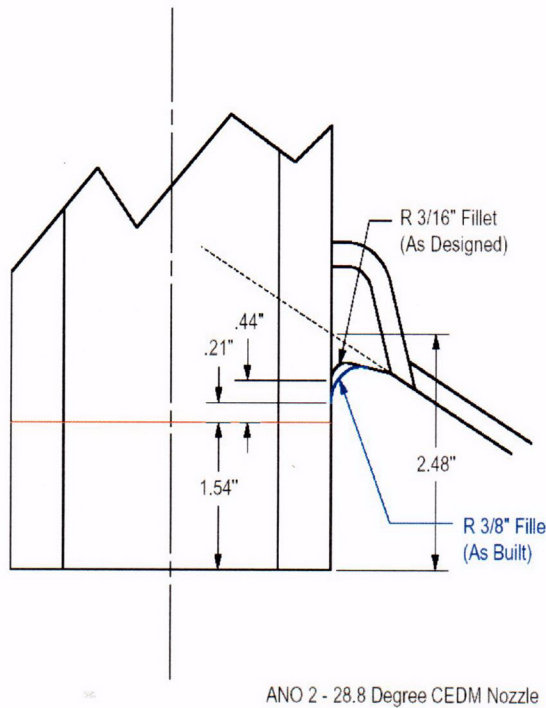| 28.8° Nozzle		Bottom		Top		Length	
		Measured	Diff	Measured	Diff	Measured	Diff
Nozzle 30	Low HS	0.16	-0.28	1.36	-0.28	1.20	0.01
	High HS	2.48	-0.21	3.76	-0.33	1.28	-0.12
Nozzle 31	Low HS	0.20	-0.24	1.32	-0.32	1.12	-0.07
	High HS	2.56	-0.13	3.56	-0.53	1.00	-0.40
Nozzle 32	Low HS	0.16	-0.28	1.24	-0.40	1.08	-0.11
	High HS	2.60	-0.09	3.64	-0.45	1.04	-0.36
Nozzle 33	Low HS	0.00	-0.44	1.40	-0.24	1.40	0.21
	High HS	2.24	-0.45	3.72	-0.37	1.48	0.08
Nozzle 34	Low HS	0.20	-0.24	1.08	-0.56	0.88	-0.31
	High HS	2.12	-0.57	3.68	-0.41	1.56	0.16
Nozzle 35	Low HS	0.16	-0.28	1.40	-0.24	1.24	0.05
	High HS	2.76	0.07	3.88	-0.21	1.12	-0.28
Nozzle 36	Low HS	0.04	-0.40	1.60	-0.04	1.56	0.37
	High HS	2.48	-0.21	3.80	-0.29	1.32	-0.08
Nozzle 37	Low HS	0.24	-0.20	1.52	-0.12	1.28	0.09
	High HS	2.68	-0.01	4.00	-0.09	1.32	-0.08

1) Differences between the bottom and top locations are varied.
2) At the downhill (low HS) location the differences between the bottom and top are significant.
3) At the uphill (High HS) location the differences are not very significant.
4) This indicates that the weld profile at the down hill location are different from that at the uphill location.
5) Experience from another CE fabricated RV head indicated that the Fillet weld at the downhill location had a larger radius than specified (¾ as found vs. 3/16 as-specified).
6) The weld size at the uphill location is close to the as-designed condition.
7) The nozzle lengths appear to be close to the as-designed value of 2.48 inches.
8) A nozzle configuration having a as-designed length, as-designed weld profile at the uphill location, and a larger fillet radius at the downhill location will minimize the observed differences between the as-designed and UT (as-measured) data.

49.6° Nozzle Group

49.6° Nozzle		Bottom		Top		Length	
		Measured	Diff	Measured	Diff	Measured	Diff
Nozzle 70	Low HS	0.00	-0.21	1.44	-0.07	1.44	0.14
	High HS	5.04	-0.01	6.52	-0.23	1.48	-0.23
Nozzle 71	Low HS	0.00	-0.21	1.32	-0.19	1.32	0.02
	High HS	5.04	-0.01	6.52	-0.23	1.48	-0.23
Nozzle 72	Low HS	0.00	-0.21	1.32	-0.19	1.32	0.02
	High HS	5.08	0.03	6.52	-0.23	1.44	-0.27
Nozzle 73	Low HS	0.00	-0.21	1.20	-0.31	1.20	-0.10
	High HS	5.00	-0.05	6.44	-0.31	1.44	-0.27
Nozzle 74	Low HS	0.00	-0.21	1.20	-0.31	1.20	-0.10
	High HS	5.12	0.07	6.28	-0.47	1.16	-0.55
Nozzle 75	Low HS	0.00	-0.21	1.20	-0.31	1.20	-0.10
	High HS	5.00	-0.05	6.40	-0.35	1.40	-0.31
Nozzle 76	Low HS	0.00	-0.21	1.60	0.09	1.60	0.30
	High HS	4.64	-0.41	6.52	-0.23	1.88	0.17
Nozzle 77	Low HS						
	High HS						
Nozzle 78	Low HS	0.00	-0.21	1.48	-0.03	1.48	0.18
	High HS	5.16	0.11	6.68	-0.07	1.52	-0.19
Nozzle 79	Low HS	0.00	-0.21	1.64	0.13	1.64	0.34
	High HS	4.96	-0.09	6.52	-0.23	1.56	-0.15
Nozzle 80	Low HS	0.00	-0.21	1.44	-0.07	1.44	0.14
	High HS	4.96	-0.09	6.52	-0.23	1.56	-0.15
Nozzle 81	Low HS	0.00	-0.21	1.56	0.05	1.56	0.26
	High HS	5.08	0.03	6.48	-0.27	1.40	-0.31

1) Observations are similar to that fro the 28.8° nozzle group. Therefore a similar nozzle configuration would exist.

2) The estimated as-built nozzle configuration for this group is similar to that for the 28.8° nozzle group.

3) Using this approach it is demonstrated that the weld bottom at the downhill location would fall 0.18 inch below the dead zone for this group of nozzles.

4) Sketches in the following pages show the estimated as-built configurations for the 28.8° nozzle group and the 49.6° nozzle group.

Sketches for Estimated As-Built configuration for the 28.8º and 49.6º nozzle Groups

R 3/16" Fillet
(As Designed)

.44"

.21"

2.48"

1.54"

R 3/8" Fille
(As Built)

ANO 2 - 28.8 Degree CEDM Nozzle

R 3/16" Fillet
(As Designed)

.21"

1.54"   .18"

2.48"

R 3/8" Fillet
(As Built)

ANO 2 - 49.6 Degree CEDM Nozzle

Sketches showing estimated as-built configurations. The blue lines show the estimated as-built profiles for the weld (fillet cap) at the downhill locatrion.

C30